Mapping submarine glacial landforms using acoustic methods

M. JAKOBSSON[1]*, R. GYLLENCREUTZ[1], L. A. MAYER[2], J. A. DOWDESWELL[3], M. CANALS[4], B. J. TODD[5], E. K. DOWDESWELL[3], K. A. HOGAN[6] & R. D. LARTER[6]

[1]*Department of Geological Sciences, Stockholm University, Svante Arrhenius väg 8, 106 91 Stockholm, Sweden*

[2]*Center for Coastal and Ocean Mapping, University of New Hampshire, Durham, New Hampshire 03824, USA*

[3]*Scott Polar Research Institute, University of Cambridge, Cambridge CB2 1ER, UK*

[4]*GRC Geociències Marines, Universitat de Barcelona, 08028 Barcelona, Spain*

[5]*Geological Survey of Canada, Natural Resources Canada, PO Box 1006, Dartmouth, Nova Scotia B2Y 4A2, Canada*

[6]*British Antarctic Survey, Natural Environment Research Council, High Cross, Madingley Road, Cambridge CB3 0ET, UK*

**Corresponding author (e-mail: martin.jakobsson@geo.su.se)*

The mapping of submarine glacial landforms is largely dependent on marine geophysical survey methods capable of imaging the seafloor and sub-bottom through the water column. Full global coverage of seafloor mapping, equivalent to that which exists for the Earth's land surface, has, to date, only been achieved by deriving bathymetry from radar altimeters on satellites such as GeoSat and ERS-1 (Smith & Sandwell 1997). The horizontal resolution is limited by the footprint of the satellite sensors and the need to average out local wave and wind effects, resulting in a cell size of about 15 km (Sandwell *et al.* 2001). A further problem in high latitudes is that the altimeter data are extensively contaminated by the presence of sea ice, which degrades the derived bathymetry (McAdoo & Laxon 1997). Consequently, the satellite altimeter method alone is not suitable for mapping submarine glacial landforms, given that their morphological characterization usually requires a much finer level of detail. Acoustic mapping methods based on marine echo-sounding principles are currently the most widely used techniques for mapping submarine glacial landforms because they are capable of mapping at a much higher resolution.

Although the accuracy and resolution of echo-sounding methods are continually being improved, the portion of the world's ocean floor that has been acoustically surveyed is increasing only slowly. This lack of coverage is particularly true for those areas of the oceans covered by sea ice and infested with icebergs, where glacial landforms are an abundant component of continental shelf and fjord morphology. This is illustrated by the fact that only about 11% of the Arctic Ocean had been mapped using modern multibeam sonar technology by 2012 when the latest International Bathymetric Chart of the Arctic Ocean (IBCAO) was compiled (Jakobsson *et al.* 2012). A similar estimate of the mapped portion of the seafloor south of 60° S, made during the compilation of the International Bathymetric Chart of the Southern Ocean (IBCSO), yielded 15% coverage (Arndt *et al.* 2013). The use of echo sounders installed on ice-breakers and submarines and deployed on autonomous underwater vehicles (AUVs) has a relatively short history in the polar oceans (e.g. Wadhams 1978; Newton 2000). Even so, the proportion of the entire world ocean that has been mapped by echo-sounding data is not much greater than that of the polar seas. Only 18% of the 30 arc-second large grid cells of the most recent global grid for the General Bathymetric Chart of the Oceans, released in 2015, are constrained by depth measurements (Weatherall *et al.* 2015). This percentage includes any kind of sounding control point, implying that if only the portion mapped using modern multibeam methods is considered, then there may be little more of the world ocean floor surveyed than in the polar oceans.

This part of the *Atlas of Submarine Glacial Landforms* provides brief descriptions of the most commonly applied acoustic mapping methods used elsewhere in this book, their capabilities, limitations and typical errors. It begins with an introduction to how the use of acoustic geophysical survey methods has evolved within the field of marine glacial landform mapping. More details on marine geophysical mapping methods are available in textbooks on this subject (e.g. Urick 1983; Jones 1999; Wille 2005; Lurton 2010).

Efforts have been made in this contribution to illustrate some of the more common artefacts that occur when applying echo-sounding survey methods because these may interfere with the imaging and interpretation of submarine glacial landforms. Examples of mapped glacial landforms from earlier acoustic studies are shown, in addition to the more recent results presented in this *Atlas*. The examples used here, and others found throughout the *Atlas*, illustrate the recent technological developments in acoustic seafloor mapping in which the advent of multibeam systems represents, without doubt, a major technological leap forward for marine landform mappers by providing both detailed bathymetric information and insights into the surficial composition of the seafloor from backscatter data.

Development of acoustic methods applied to mapping submarine glacial landforms

The marine echo sounder was initially developed during the first part of the twentieth century (Vogt & Tucholke 1986). Between 1925 and 1927 the German research vessel *Meteor* completed 14 echo-sounding profiles across the South Atlantic. These profiles constitute the first explicit scientific use of echo-sounding methods and revealed to the scientific community how rugged the morphology of the seafloor could be. However, echo sounders were not used widely on research ships until about a decade after the Second World War. Early applications of single-beam echo sounders (SBESs) to investigate the morphology of the seafloor resulted in some of the first scientific breakthroughs in our understanding of the ocean basins and were fundamental to the development of the theory of plate tectonics (Heezen *et al.* 1959).

Single-beam echo-sounding data are not optimal for glacial landform mapping because only a line of seafloor depth soundings, averaged over a typically broadbeam footprint beneath the ship, is acquired as the ship moves forwards. Despite this, pioneering scientific work deployed SBESs on glaciated continental margins to provide important new insights about submarine glacial landforms and palaeo-ice sheet activity (e.g. Hunkins *et al.* 1962; King 1969; Holtedahl & Sellevoll 1971; Damuth 1978). Because an individual SBES profile provides seafloor relief only along a one-dimensional profile, linear features on the seafloor, such as iceberg ploughmarks, can be discerned if crossed and of a large enough scale (Fig. 1a, b). However, to obtain the two-dimensional (2D) view required to study ploughmark directions, multiple adjacent lines must cross the feature to construct bathymetric contour maps. The considerable time and effort required to collect closely spaced

From: Dowdeswell, J. A., Canals, M., Jakobsson, M., Todd, B. J., Dowdeswell, E. K. & Hogan, K. A. (eds) 2016. *Atlas of Submarine Glacial Landforms: Modern, Quaternary and Ancient*. Geological Society, London, Memoirs, **46**, 17–40, http://doi.org/10.1144/M46.182

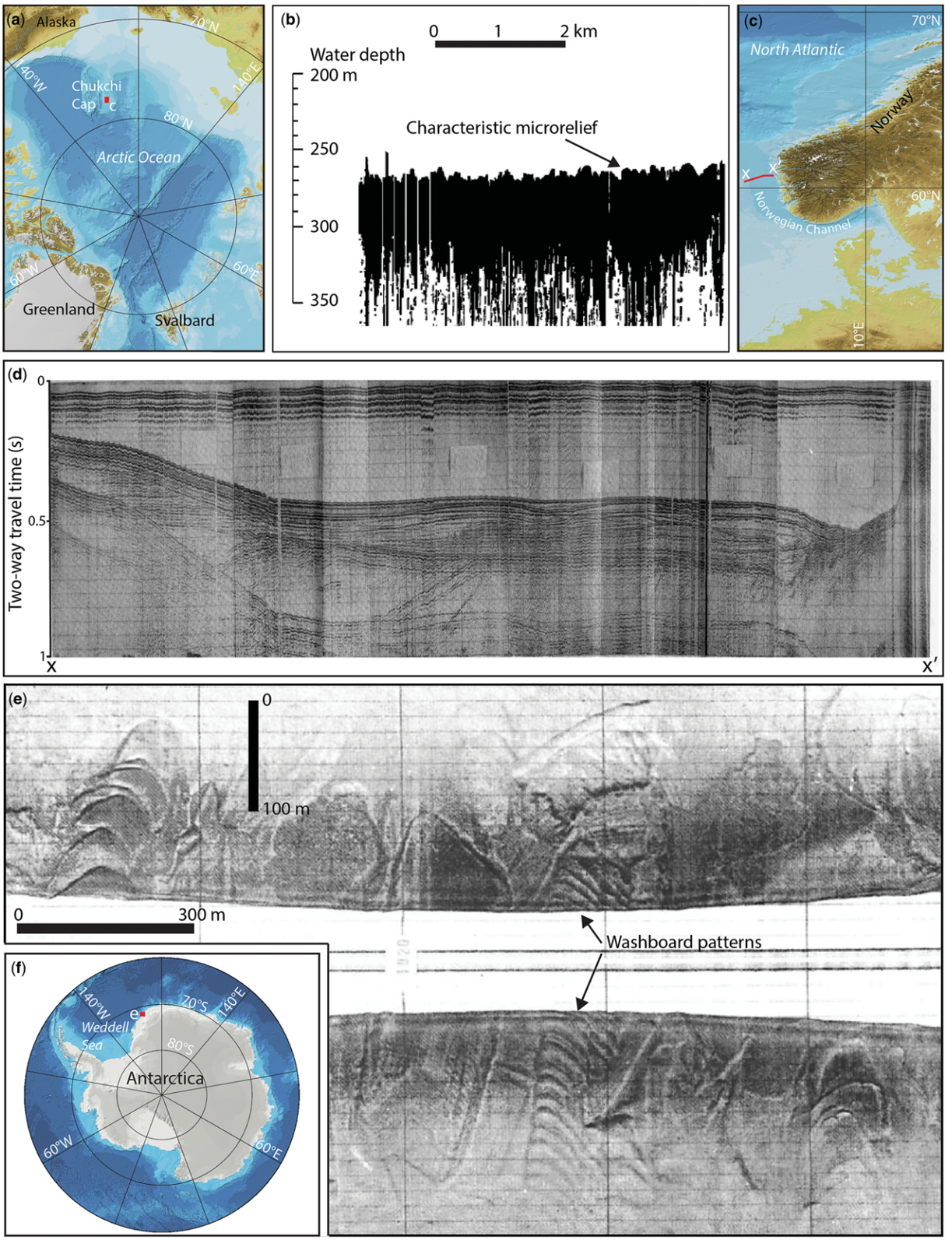

Fig. 1. Examples of the first seafloor and sub-seafloor acoustic mapping records used to interpret submarine glacial landforms. (**a**) Location map showing where the SBES profile in (c) was acquired on the crest of the Chukchi Cap, central Arctic Ocean (map from IBCAO v. 3.0). (**b**) Bathymetric profile collected from the drifting ice station *Charlie* in 1959 with a 1.8 kHz SBES developed at Lamont Doherty Earth Observatory (data from Hunkins *et al.* 1962). The seafloor relief was interpreted to be caused by the ploughing action of iceberg keels, which has since been confirmed by more modern MBES data (Polyak *et al.* 2001; Jakobsson *et al.* 2005; Dove *et al.* 2014). (**c**) Location map of seismic-reflection profile (red line, x–x′) shown in (d) from the Norwegian Channel (map from GEBCO_08). (**d**) Seismic-reflection profile collected in the early 1970s and interpreted to show that the Norwegian Channel had been shaped primarily by palaeo-ice stream activity (seismic-reflection data from Sellevoll & Sundvor 1974; length scale is not provided in original publication). (**e**) Side-scan sonar image acquired in the mid-1970s off Wilkes Land in the Weddell Sea, Antarctica, showing features referred to as washboard patterns and interpreted to be caused by the tidal motions of grounded icebergs (side-scan imagery from Lien 1981). (**f**) Map of Antarctica locating the side-scan sonar image in (e) (from IBCSO v. 1.0). Acquisition system Klein Model 400. Frequency 100 kHz.

echo-sounding profiles, together with the labour-intensive post-processing needed to compile bathymetric contour maps, delayed the publication of detailed portrayals of submarine glacial landforms until new mapping methods were developed.

Applying the same principles as echo sounding, but using lower frequencies capable of imaging the stratigraphy hundreds of metres below the seafloor, the seismic-reflection method was developed along with echo sounding (Reddy 2012). Marine geophysical methods in the 1960s and 1970s were comparatively more advanced in the characterization of the sub-bottom stratigraphy than in imaging details of the seafloor morphology. This development was largely driven by the demands of the offshore hydrocarbon exploration industry to acquire knowledge about the sub-bottom geology that could reveal potential oil and gas reservoirs. Seismic-reflection profiles collected for exploration purposes also provided information on the glacial history of mid- and higher-latitude continental margins. For example, it was recognized from seismic-reflection data acquired during the early 1970s that the Norwegian Channel had been formed primarily through erosion by a Quaternary palaeo-ice stream (Sellevoll & Sundvor 1974) (Fig. 1c, d). The fact that the sedimentary stratigraphy of continental margins is controlled largely by the local sea-level, which, on a global basis, is related to eustatic sea-level changes through glacial–interglacial cycles, was also recognized from investigations of seismic-reflection profiles (Vail *et al.* 1977).

Side-scan sonar equipment, which provides images of the seafloor, was initially developed during the early 1950s as a military surveillance tool under conditions of some secrecy (Stride 1992). Early sonar systems were limited by analogue electronics and the technology of paper recorders. The first side-scan sonar systems produced a simple amplitude-modulated printed image of the strength of the acoustic return as a function of the travel time across the ensonified swath of seafloor, but there was no straightforward way to adjust the side-scan signal for a seafloor with bathymetric variations. Early side-scan sonar records were therefore difficult to interpret geologically, but the low incidence angles produced when systems were towed near the seafloor resulted in clear acoustic shadows being cast by bottom features. The imagery produced, often referred to as shadowgraphs or sonographs (Belderson *et al.* 1972), proved to be very useful for the identification of objects such as wrecks and mines, and therefore, side-scan sonar was, for many years, the primary system used to view and locate objects on the seafloor (Fish & Carr 2001).

The first geological applications of side-scan sonar data in the late 1950s and early 1960s included the acquisition of seafloor imagery to map the distribution of sediments (using bedform distribution and relative backscatter levels), faults and other geological structures (Stride 1960), and to extrapolate outcropping stratigraphic boundaries on the seafloor for the production of geological maps (Donovan & Stride 1961). The development of a commercial side-scan sonar system was begun at the Massachusetts Institute of Technology by Harold Edgerton and Martin Klein. They had a side-scan sonar system built in 1963–64 by the company EG&G (Edgerton, Germeshausen and Grier Inc.), which was mounted on the submersible *Trieste* (Geyer 1977).

Although side-scan sonar can complement SBESs by providing textural information on the seabed between ship tracks, it is commonly installed and deployed in a tow-fish, resulting in an additional challenge to deployment in high-latitude environments where sea ice is often present. However, when used on formerly glaciated continental margins devoid of modern sea ice, the 2D nature of side-scan imagery immediately provided useful information on submarine glacial landforms. Interactions between icebergs and the seafloor were revealed with much greater detail in side-scan imagery compared with the results that had been possible using SBESs or seismic-reflection profiling (Belderson & Wilson 1973; Harris & Jollymore 1974; Barrie 1980; Klepsvik & Fossum 1980; Lien 1981). This is exemplified by side-scan records acquired in the Weddell Sea, Antarctica during the Norwegian Antarctic Research Expedition of 1976–77 (Lien 1981) (Fig. 1e, f). Regular patterns of small ridges at the base of iceberg ploughmarks, referred to as washboard patterns, were identified in this part of the Antarctic continental shelf and a mechanism for their formation was proposed based on the side-scan imagery (Lien 1981; Barnes & Lien 1988). Records collected using a side-scan sonar system deployed through a sonar trunk in the hull of RRS *Discovery* off the northern Antarctic Peninsula in 1984–85 revealed a progression of glacial bedform types that became more elongate with increasing distance offshore (Pudsey *et al.* 1994). By the early 1980s side-scan sonar technology had advanced to include the use of multiple rows of transducers and interferometric or phase-measuring processing that allowed the seafloor depth to be acquired together with backscatter information (Blackington *et al.* 1983).

Accurate high-resolution depth measurements were the target for the next development in sonar technology: the multibeam echo sounder (MBES) (Tucker 1961; Renard & Allenou 1979). Similar to side-scan sonar, the MBES was first developed for military purposes under high secrecy. Spearheading this development was a US company, General Instruments (later SeaBeam Instruments, which is now part of ELAC Nautik in the L-3 Communications Group), who developed a technique for the US Navy that was capable of producing several narrow-beam depth soundings from a single vessel. The technique became known as Sonar Array Sounding Systems (Farr 1980). In 1977, the original SeaBeam system was developed from military experiences and became the first commercially available MBES (Farr 1980). The first SeaBeam system had 16 beams capable of imaging a sector of 90° beneath the vessel. The Norwegian company Simrad, at the time specializing in fish-finding echo sounders, formed a hydrographic division in 1975. Under a development contract with the Norwegian oil company Statoil, Simrad began working on their first multibeam system, the Simrad EM 300 (operating at 300 kHz). This project came close to a solution, but suffered from working with a frequency that was higher than could be handled efficiently at that time. The experience gained, however, was brought into the next development project with Hans M. Gravdal, who needed an efficient bathymetric mapping device for his survey company Geoconsult. Together they began development of the Simrad EM100 (100 kHz), which was introduced commercially in 1986 with a configuration consisting of 32 beams over a swath width of 100°.

Although the first civilian applications of MBESs in the 1980s and 1990s were dominated by the needs of the offshore hydrocarbon industry, the potential for using MBESs for the dimensional characterization of submarine landforms was soon realized by marine geologists. Among the pioneering uses of MBESs to map submarine glacial landforms was a survey east of Halifax, Canada published by Loncarevic *et al.* (1994). They used the early Simrad EM100 to map a 1000 km^2 area where several classical glacial landforms, such as ribbed moraines and drumlins, were identified. Sets of mega-scale glacial lineations were imaged comprehensively for the first time off the northern Antarctic Peninsula during the austral summer of 1996–97 using a Simrad EM12S system (Canals *et al.* 2000).

A key advantage of multibeam sonar is that it provides the full 2D spatial distribution of depths across a swath of seafloor along with backscatter information, both of which provide insights into the formation mechanisms behind many submarine glacial landforms. As an example, the extremely regular features imaged using side-scan sonar by Lien (1981) in the Weddell Sea, Antarctica were later mapped using modern MBESs in Pine Island Bay, West Antarctica (Fig. 2) (Jakobsson *et al.* 2011; Jakobsson & Anderson 2016) and north of Svalbard (Dowdeswell & Hogan 2016). The formation mechanism behind these features, called corrugation ridges, may be linked to the tidal motion of icebergs; the detailed bathymetric information provided by the multibeam system allowed a suite of statistical analyses of the depth

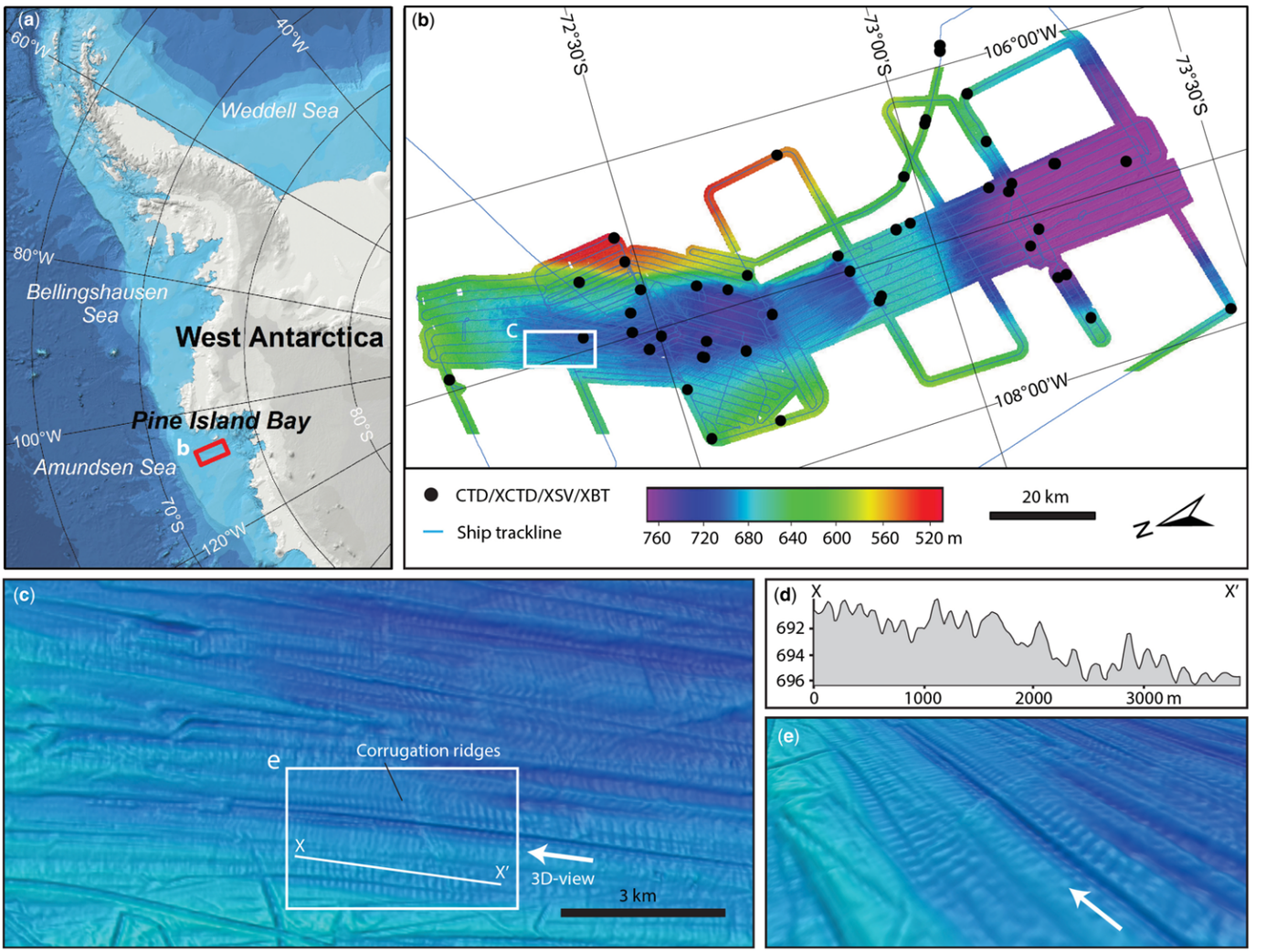

Fig. 2. Results from mapping with a modern MBES system deployed from the Swedish icebreaker *Oden* in Pine Island Bay, West Antarctica. Multibeam acquisition system Kongsberg EM 122. Frequency 12 kHz. Grid-cell size 15 m. (**a**) Map showing the location of the multibeam imagery in (b) (from IBCAO v. 3.0). (**b**) Detailed map of the ship tracks and core sites (black dots) acquired during the *Oden* survey in Pine Island Bay. (**c, e**) Detailed multibeam images of the seafloor features referred to as corrugation ridges (Jakobsson *et al.* 2011). The spatial dimensions of these regular corrugation ridges were analysed statistically and the formation mechanism was linked to tidal motion of icebergs from a disintegrated ice shelf–ice stream system. (**d**) Bathymetric profile between X and X′ in (c) extracted from the MBES data. VE × 121.

dimension not possible with a side-scan image alone (Jakobsson *et al.* 2011). The study from Pine Island Bay also demonstrated that the resolution of the acquired bathymetry can be of crucial importance. The areas with the corrugation ridges had been passed over previously by research vessels equipped with multibeam technology, but it was only after a systematic survey with 100% overlapping swaths and regular sound-speed control, using the best deep water multibeam technology available at the time, that the small corrugation ridges, only a few metres high, were identified. The survey was carried out in 2010 in an unusually ice-free Pine Island Bay with the Swedish ice-breaker *Oden*, which had been upgraded from a Kongsberg EM120 (1° × 1°, 12 kHz) to an EM122 system with enhanced resolution; specifically, the along-track resolution was enhanced by the implementation of dual swaths where a second swath was transmitted at an angle away from the first to increase the along-track resolution of the ensonified seafloor.

To achieve higher resolution imagery of the seafloor in deep water than is possible from surface vessels equipped with low-frequency (*c.* 12 kHz) deep-water MBESs, high-resolution shallow-water systems have been mounted on AUVs that are capable of navigating close to the seafloor at considerable water depths (e.g. Dowdeswell *et al.* 2008). AUVs are also able to map areas unreachable by surface vessels – for example, underneath floating ice shelves. Corrugation ridges were mapped beneath the ice shelf of the Pine Island Glacier using a Kongsberg EM2000 (200 kHz) mounted on the AUV *Autosub3* (Graham *et al.* 2013).

The high-resolution depiction of submarine glacial landforms provided by multibeam sonar can be continued into the subsurface through the use of a sophisticated seismic technique known as three-dimensional (3D) seismic imaging. The first offshore 3D seismic survey was completed near Houston in 1967 by Exxon (Cleveland & Morris 2014). 3D seismic surveys are very expensive and therefore most surveys are carried out for offshore hydrocarbon exploration purposes; however, 3D seismic datasets acquired by industry are sometimes shared for basic research applications. In addition, some high-resolution 3D seismic systems, such as P-Cable, are increasingly being deployed by the academic community. This *Atlas* contains several examples of 3D seismic data, initially collected for hydrocarbon exploration, that have been used to interpret the submarine glacial landform record (e.g. Dowdeswell & Ottesen 2016; Stewart 2016; Vadakkepuliyambatta *et al.* 2016).

The ability to move beneath the seafloor and extract old buried seafloor surfaces for morphological interpretation provides particularly strong potential for the use of 3D seismic information when reconstructing the glacial history of a region (e.g. Dowdeswell *et al.* 2006; Andreassen *et al.* 2007).

Bringing data together: 3D visualization

The development of computer 3D visualization techniques has provided powerful new methods for the integration of geological and geophysical information. Digitization was, however, a necessary initial step before computer visualization could be implemented because the early geophysical data acquisition systems were all analogue. The first digitizing table was specifically designed by Swedish inventor Håkan Lans in the 1970s to digitize reflectors on seismic profiles. The invention was named 'the digitizer' and later HI-Pad after it was bought by Houston Instruments. The digitizer could be used to trace the seafloor on analogue echo-sounding records, as well as for digitizing regular maps.

Beginning in the mid-1980s, software for the 3D visualization of multibeam bathymetry, along with other geo-information about the composition of the seafloor, such as backscatter, was developed by the Ocean Mapping Group at the University of New Brunswick, Canada. A specific effort was made to provide a '3D feeling' for the seafloor morphology using an enhanced version of the hill-shading technique referred to as cast shadows (Ware 1989). This has proved to be a particularly useful visualization technique when interpreting submarine glacial landforms in multibeam-swath bathymetric data. The rendering algorithms and the methods for the interaction of users with the geophysical data were developed at the Ocean Mapping Group by Colin Ware. These were incorporated into the 3D visualization software that is today widely used by marine geologists (Mayer *et al.* 2000).

An illustration of how multibeam bathymetry, side-scan sonar, sub-bottom acoustic and seismic-reflection profiles can be merged into a digital 3D environment for geological interpretation is shown in Figure 3. Adding ground-truth geological information from shallow sediment coring and deep drilling is also common in both industrial and scientific applications.

Principles of seafloor and sub-seafloor acoustic mapping methods

This section provides a brief overview of the principles behind acoustic mapping methods based on echo sounding. The purpose is to provide some of the basic background needed for an understanding of the physics of acoustic reflections and how such reflections are used in the mapping of both the seafloor and sub-bottom. In particular, these simple principles lay the foundation for a further discussion on acoustic artefacts in acquired seafloor mapping data. Such geophysical artefacts commonly cause problems when interpreting seafloor morphology and/or sub-bottom geology.

Echo sounding

The basic principle of echo sounding is to transmit a sound pulse using an acoustic source and to measure accurately and precisely the time it takes for the pulse to return after being reflected off the seafloor. Although this principle is shared by SBESs, MBESs, side-scan sonar systems, sub-bottom profilers and by seismic-reflection profiling, there are considerable differences in the detailed mechanisms, errors and interpretation possibilities of these methods. Before we describe the individual methods in more detail, as well as the key parameters associated with their collection and interpretation, the fundamental common characteristics of the methods are described.

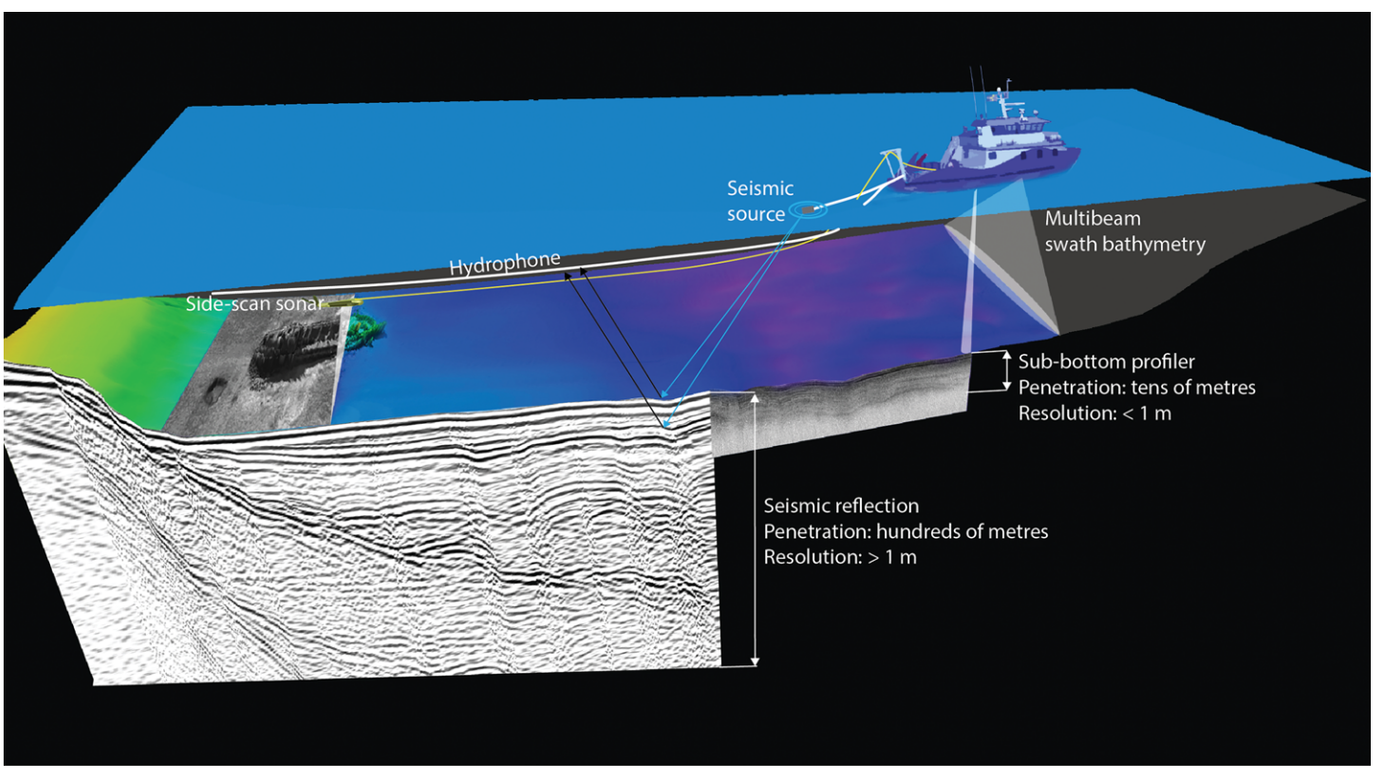

Fig. 3. Multibeam bathymetry, side-scan sonar, sub-bottom and seismic-reflection profiling information brought together in a 3D environment for geological interpretation.

The basic principle of echo sounding is simple: a sound source (also called a transmitter, projector or Tx) transmits a sound pulse (ping) into the water at a known time. The sound pulse is reflected (echoed) from the seafloor or other targets and the time of its return is recorded by a receiver (Rx). The two-way travel time (TWT) is then calculated. Given that the speed of sound through the water column (v) can be measured, the TWT may be converted to local depth (D) as:

$$D = v \times \frac{\mathrm{TWT}}{2}. \quad (1)$$

The sound source and receiver in SBESs, MBESs and side-scan sonar systems are usually made from piezoelectric ceramic materials. Seismic systems commonly apply one of several methods to generate a sound wave (e.g. compressed air, compressed water or sparks) and they use so-called streamers with hydrophones of piezoelectric material to receive the returned signal. Piezoelectric materials are transducers that convert electrical energy into mechanical energy, resulting in a sound pulse (pressure wave). Conversely, when a pressure wave impinges on a piezoelectric transducer, an electrical current is generated. For SBESs, including simple sub-bottom profilers and side-scan sonar systems, the same transducer (often consisting of multiple elements) is commonly used both as the source and receiver. MBESs, more sophisticated phase-measuring side-scan sonar systems and seismic-reflection systems are based on designs where the source and receiver use different transducers, sometimes physically separated.

Reflection and refraction

When a sound wave meets an interface between two materials that have different sound speeds and/or densities, some of the energy is reflected at the interface with the same angle as the angle of incidence and some continues to propagate into the second medium (Fig. 4a). If the angle of incidence is oblique, a portion of the wave is refracted (bent) at the interface and continues to propagate through the lower material at an angle that is described by Snell's law:

$$\frac{\sin\theta_1}{v_1} = \frac{\sin\theta_2}{v_2} \quad (2)$$

where θ_1 is the incident angle (away from normal) and θ_2 is the angle of refraction. The different speeds of sound in the materials are denoted as v_1 and v_2, respectively (Leenhardt 1972). Refraction is not only encountered in acoustics; it is a widespread

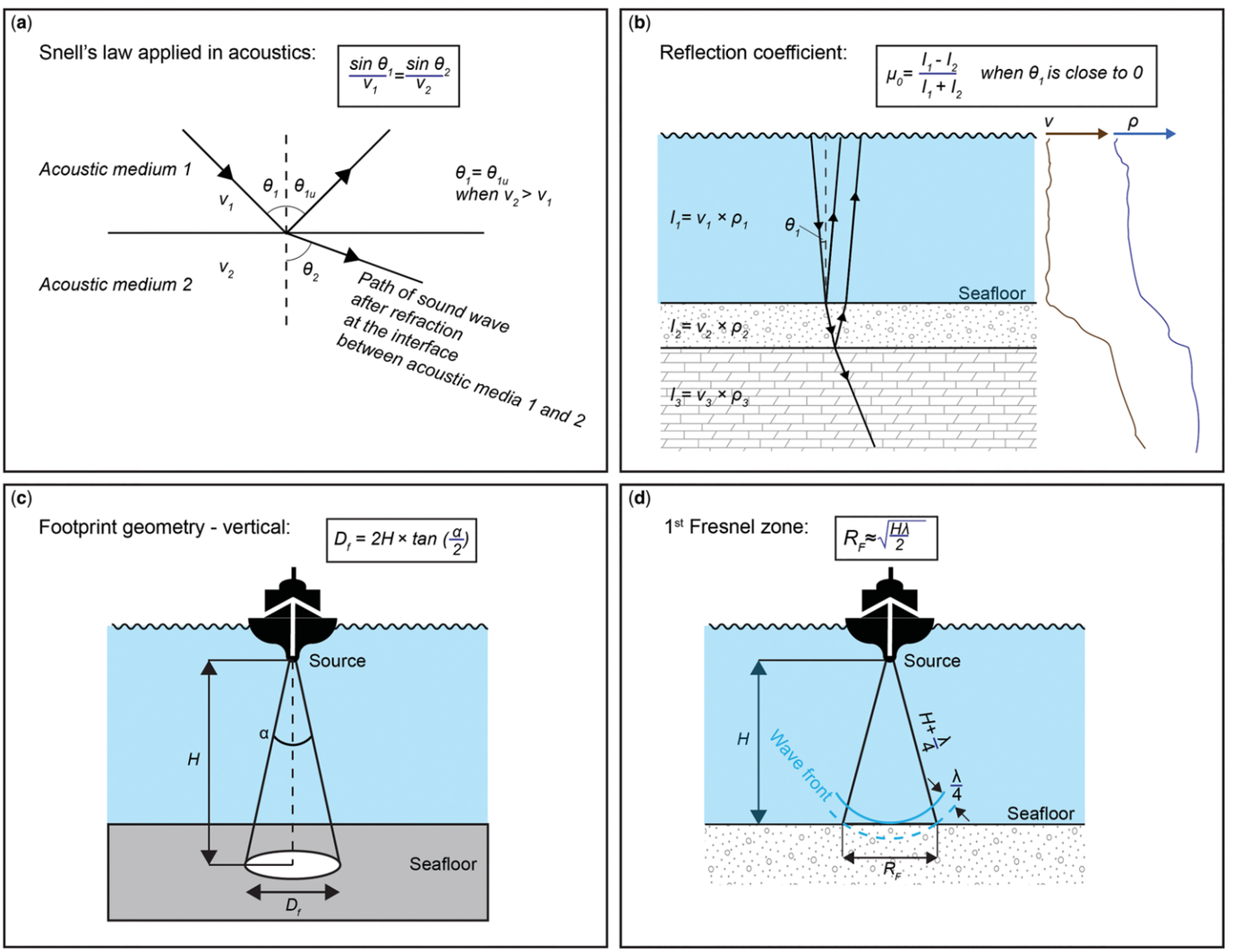

Fig. 4. Schematic illustrations of acoustic principles. (**a**) Snell's law as applied in acoustics. (**b**) Calculation of reflection coefficients between acoustic media of different acoustic characteristic impedance (I). (**c**) Footprint geometry of a vertical beam. (**d**) First Fresnel zone.

phenomenon in optics where light rays hit a boundary between two media – for example, air and water. This phenomenon is most commonly displayed when white light enters a prism and is refracted into its component colours.

Decibel scale

Sound levels are measured with a logarithmic decibel (dB) scale. The decibel scale facilitates the comparison of numbers over several orders of magnitude and is used for all calculations involving sound levels – for example, to establish signal-to-noise ratios (SNRs) using the sonar equation. The sound pressure level (L, dB) is defined by comparing the intensity or power of the sound (I, W m^{-2}) with a reference value (I_0, W m^{-2}), where

$$L = 10 \log \frac{I}{I_0}. \quad (3)$$

The reference pressure for underwater sound is 1 μPa measured 1 m away from the source. It should be noted that the standard reference pressure in air is 20 μPa at 1 m distance to facilitate comparison of the sound level with human perception. Sound levels expressed in decibels must therefore include the reference pressure and decibel levels in water and air cannot be compared directly. The decibel scale implies that a change in power ratio by a factor of ten is a 10 dB change and a change in power ratio by a factor of two is a *c.* 3 dB change.

Sonar equation

The sonar equation simplifies and describes each of the factors involved in the acoustic echo-sounding process. It is an energy budget expression used to calculate SNRs and to optimize sonar systems during installation and for testing and predicting sonar performance. The equation provides the signal excess (*SE*), commonly referred to as the reception threshold (*RT*) in the ocean mapping case, which is the strength of the measured echo return with respect to an expected level of performance in decibels. All quantities are given in units of decibels. Several versions of the sonar equation exist, depending on the purpose and level of specification needed. The form given here is for the generic case of an active sonar system (described further in Lurton 2010):

$$RT = SL - 2TL + TS - NL + DI + PG. \quad (4)$$

The source level (*SL*) is the amount of energy from the transducer, measured as the level of the acoustic signal intensity at 1 m from the centre of the source transducer. The transmission loss (*TL*) is the loss of energy from attenuation (the conversion of mechanical energy to heat), mostly through the influence of dissolved salts and from geometric spreading. These losses occur twice – first as the transmitted pulse propagates towards the seafloor and again when the reflected pulse travels back towards the receiver. The target strength (*TS*) is the ratio between the reflected and the transmitted intensities and depends on the impedance contrast and surface roughness of the target. The noise level (NL) is the total contribution from external ambient noise and internal noise in the sonar system. Because only a true point source would have pure spherical spreading, the directivity index (*DI*) accounts for the actual beam shape of the sound, defined as the ratio between the non-directional intensity and the directional intensity. The processing gain (*PG*) is the amplification of the signal, which may be performed at the receiver.

The fundamental measurement of the echo sounder is the TWT, which can be converted to range or depth with appropriate information about the speed of sound through the water column. In addition, side-scan sonar and multibeam sonar systems also have the capability to measure the amplitude of the returned echo, sometimes known as the backscatter strength. Backscatter depends on the angle of incidence as well as the acoustic impedance contrast (the product of the speed of sound and the saturated bulk density) between the water and the seafloor material. Relative changes in backscatter are used to infer changes in seafloor materials; more quantitative analyses of backscatter may also be used for seafloor characterization studies (Fonseca & Mayer 2007). A geological material that yields high backscatter values is thus a material of high target strength (*TS*) as defined in the sonar equation (equation 4).

Importance of sound speed

In any fluid, the propagation speed of pressure waves, such as sound, is governed by two physical quantities: the fluid's density and the bulk modulus (i.e. its compressibility). The sound speed (v) is calculated using the bulk modulus (K) and the density (ρ) as:

$$v = \sqrt{\frac{K}{\rho}}. \quad (5)$$

The speed of sound thus increases with decreasing compressibility (larger bulk modulus), but decreases with increasing density. The compressibility and density obviously vary greatly in different seafloor and subsurface geological materials, but there is also significant variation in the properties of the water column depending on the temperature, pressure and dissolved impurities (mostly expressed as salinity). In freshwater at 25°C, sound travels at about 1497 m s^{-1}. Colder freshwater has a higher density and therefore a lower sound speed, down to 4°C where freshwater has its maximum density, other factors being equal. It should be noted, however, that salinity fluctuations in saline ocean water change the density–temperature relationship so that the maximum density may no longer be at 4°C.

Water layers with different sound speeds cause refraction of the non-vertically incident sound waves following Snell's law (equation 2) (Fig. 4a). This means that a sound pulse travelling down at an oblique angle will bend out towards the horizontal when passing from a lower speed layer into a higher speed layer; it will bend down towards the vertical on going from a higher speed layer to a lower speed layer. Therefore a knowledge of the sound velocity profile (SVP) of the water column is crucial for accurate results in any type of echo sounding. This is discussed further when the topic of acoustic artefacts is addressed. An SVP through the water column is usually obtained either by measurement of the sound speed directly, or is calculated from measurements of the temperature, salinity and pressure through the water column. The SVP is usually measured using a conductivity–temperature–depth probe deployed on a cable from the parent ship or with expendable probes. Several formulae with different validity ranges exist for calculating the sound speed (v, m s^{-1}) based on temperature (T, °C), salinity (S, ppt) and pressure (D, depth, m). One of the most commonly used is the empirically derived Mackenzie formula (Mackenzie 1981):

$$\begin{aligned} v = {} & 1448.96 + 4.591T - (5.304 \times 10^{-2})T^2 + (2.374 \times 10^{-4})T^3 \\ & + 1.340(S - 35) + (1.630 \times 10^{-2})D + (1.675 \times 10^{-7})D^2 \\ & - (1.025 \times 10^{-2})T(S - 35) - (7.139 \times 10^{-13})TD^3. \end{aligned} \quad (6)$$

This equation is valid in water temperatures of 2–30°C, salinities of 25–40 ppt and depths of 0–8000 m. From equation (6), we see that the sound speed increases by about 1.3 m s^{-1} per 1 ppt of increase in salinity, by about 1.7 m s^{-1} for every 100 m increase in water depth and non-linearly by about 2.5–4.7 m s^{-1} for each degree Celsius of increase in temperature.

For all echo-sounding surveys, the sound speed should ideally be sampled as densely as possible for the entire water column to construct a full sound speed profile. For multibeam surveys, good quality SVPs are an absolute requirement because sound beams at oblique angles will be refracted and their trajectories have to be calculated (ray-traced) to give accurate depth information.

For single-beam surveys and sub-bottom profiling, a harmonic mean value of the water column sound speeds is usually adequate. In a record of sound speed samples through the water column, each sample can be assumed to represent a hypothetical layer with a known sound speed, where the thickness of the layer is calculated between the midpoints of every two samples. The harmonic mean (as opposed to a simple arithmetic mean) is necessary to account for the different amounts of time the sound pulse will spend in each velocity layer. For a number of samples (n) and layer thicknesses (Δd), the harmonic mean speed (v_{harmonic}) is:

$$v_{\text{harmonic}} = \left[\frac{\sum_{i=1}^{i=n} \Delta d(i)/v(i)}{\sum_{i=1}^{i=n} \Delta d(i)} \right]^{-1}. \quad (7)$$

The calculated speed from equation (7) can then be used in equation (1) to obtain more accurate depths.

Cause of an echo: characteristic acoustic impedance

A reflection at the seafloor when using an SBES, MBES or side-scan sonar system, or at a subsurface layer when using sub-bottom profiling or seismic-reflection methods, represents a distinct vertical physical change in sound propagation properties, in particular the characteristic acoustic impedance (I). The characteristic acoustic impedance (commonly simply called impedance) is the product of the compressional sound speed (v) and the bulk density (ρ) of the material:

$$I = v \times \rho. \quad (8)$$

The amount of energy reflected from an interface is determined by the contrast in impedance between the two layers, calculated as the difference in the characteristic acoustic impedance ($I_2 - I_1$) divided by the sum of the characteristic acoustic impedances ($I_2 + I_1$). This parameter is called the reflection coefficient (μ_0) (Fig. 4b):

$$\mu_0 = \frac{I_2 - I_1}{I_2 + I_1}. \quad (9)$$

The magnitude of the changes in material properties that will result in a reflection depends on the rate of change of the properties as well as the frequency, bandwidth, beam width, the value of *SL* and the overall SNR of the sonar system. The sound speed through, and density of, the seafloor materials can be measured on discrete samples or in a sediment core using a multi-sensor core logger. Such physical property data are used as an aid in the interpretation of sub-bottom profiles, or even to calculate synthetic seismograms for optimum core-to-profile correlation. Synthetic seismograms are produced by using an algorithm that models the sound pulse as a wavelet and convolves that wavelet with the series of reflection coefficients determined from the physical properties measured along the core. The result can be compared with a real sub-bottom profile from the core location to indicate which core depths correspond to acoustic reflections (Mayer 1979).

Beam angle

A transducer within an echo sounder projects sound across its entire face. Constructive and destructive wave interference occurs close to the transducer, which constricts the sound into a conical beam. The beam angle (known as the opening angle or aperture) depends on the interference pattern, which is governed by the sound frequency and the transducer length, and is determined by the manufacturer at a certain energy level and distance from the transducer. This level varies between different manufacturers but, following the International Hydrographic Organization (2005), the beam angle (α) in degrees at the -3 dB level (half-power) can be calculated for different transducer diameters ($\emptyset$) and wavelengths (λ) as:

$$\alpha = \frac{60 * \lambda}{\emptyset}. \quad (10)$$

Several transducers mounted in an array at distances of λ (or $n \times \lambda$) will cause constructive interference of the sound waves. The sound waves act as beams along the trajectories of constructive interference, where the most focused beam (highest sound intensity) will be in the centre, which is usually directed orthogonal to the transducer face (typically vertically downward). The constructive interference will be stronger, and the beams narrower, with an increasing number of transducer elements in the array.

Footprint

When planning a survey, the ensonified area for each ping can be calculated to anticipate seafloor coverage. The ensonified area is the area of the seafloor that intersects the beam and is called the sonar footprint (Fig. 4c). For a vertical sound pulse, the footprint diameter (D_f) may be estimated based on the triangular geometry of the local water depth under the transducer (H) and the opening angle (α), as

$$D_f = 2H \times \tan\left(\frac{\alpha}{2}\right). \quad (11)$$

An array of transducers must be used to implement a directional signal transmission or reception. The length of the transducer array and applied frequency is inversely proportional to the beam width that it is possible to generate. The beam width in degrees (α_b) can be approximated by the following expression:

$$\alpha_b \approx \frac{100\,000}{(lf)} \quad (12)$$

where l is the length of the array in metres and f is the frequency in hertz. The sound beam will be narrower with increasing transducer size and higher frequency. This implies that a sonar's physical dimensions govern the achievable footprint. Long linear arrays of transducers (as used in side-scan and multibeam sonar systems), produce beams that are very narrow (typically in the along-track direction) and thus greatly aid in limiting the area of the ensonified seafloor with a consequent increase in the achievable target resolution. The attenuation (loss of energy as a function of range) increases with increasing frequency and thus a relatively low frequency is necessary to obtain the maximum range through the water column. Very large transducer arrays are required to produce a narrow beam at low frequencies (e.g. full ocean depth MBES arrays can be more than 10 m long). The array size is thus one of the limiting factors in the performance of sonar systems.

Spatial resolution

For sonar data, resolution means the minimum distance by which two objects must be separated to be recorded as distinct entities. The horizontal and vertical resolutions are governed by the smallest footprint that a transducer is capable of producing, as well as several additional factors that influence the capability of a sonar system to resolve seafloor and sub-bottom features.

Vertical resolution. When measuring depth, the vertical resolution is of paramount importance. Because the recording medium in modern sonar systems is digital, the sampling rate is not a limiting factor and thus the vertical resolution depends on the pulse length and the transmitted beam width (a narrow beam will minimize side echoes; see later discussion on artefacts). The pulse length determines the total amount of energy released at a certain power level (*SL* in equation 4). For a continuous wave (CW) pulse, a longer pulse means more energy, but a lower resolution. Two objects must be separated by more than half the pulse duration to be recorded distinctly, otherwise they will be recorded as a single object (following the Nyquist theorem; see later section on horizontal resolution). The minimum pulse length is governed by a transducer's internal resonance frequency during pulse creation and must be longer than half the period (frequency^{-1}) of the pulse. Thus higher frequencies typically result in shorter pulse lengths and greater vertical resolution. The pulse length is usually set automatically by the software for a certain transducer given the frequency and required depth range.

From this discussion, it is logical that we would want to survey with the highest frequency possible to obtain the highest vertical resolution. The use of high frequencies, however, must be traded against the absorption of sound in seawater, which is caused by the conversion of mechanical energy to heat and which takes place more rapidly at higher frequencies. Thus the range of propagation achievable by a sonar system is related directly to frequency and therefore the operating frequency of a sonar system must be selected to ensure that the maximum resolution is achieved while still maintaining the ability to propagate to the seafloor and back in a given water depth. In hull-mounted systems, higher frequencies are commonly used for shallower waters, whereas lower frequencies are needed at increasing depths, with the subsequent reduction in vertical resolution that goes with this. To achieve a better resolution in deep water, high-frequency systems can be mounted on underwater vehicles such as remotely operated vehicles (ROVs) or AUVs operating close to the deep seabed. Table 1 lists common frequencies for different sonar ranges (International Hydrographic Organization 2005) and wavelengths at 1500 m s^{-1} sound speed.

The vertical resolution (R_v) obtained is, in practice, set by the Rayleigh criterion (Kallweit & Wood 1982):

$$R_v \approx \frac{\lambda}{4} \tag{13}$$

where λ is the wavelength. This means that two objects (e.g. stratigraphic layers in a sub-bottom profile or depth differences in SBES data) must be separated vertically by at least a quarter of the wavelength to be distinguishable as separate reflections.

Ultimately, the vertical resolution of a sonar system is determined by the bandwidth (frequency range) of the transducer (*c.* 1/bandwidth). In the CW mode, the shorter the pulse length at a given frequency (as described earlier), the higher the resolution. However, sonar systems can also use a long, swept, frequency-modulated (FM) pulse that provides a larger bandwidth over the long pulse length. If the returns from such pulses are then run through a matched filter (i.e. a process of correlation that attempts to identify a replica of the outgoing pulse in the return), the processed record can achieve the resolution defined by the bandwidth of the FM pulse, but without the pulse length constraint of a CW pulse. In this way, greater propagation can be achieved while maintaining a high resolution. Modern sub-bottom profilers – for example, chirp sonars – use this technique to achieve deeper penetration beneath the seafloor, whereas some MBESs use FM pulses to maximize propagation ranges along the outer beams in deep water.

Table 1. *Common frequencies for different sonar ranges*

Depth (m)	Frequency (kHz)	Wavelength (cm)
<100	>200	<0.75
100–1500	50–200	3–0.75
>1500	12–50	12.5–3

International Hydrographic Organization (2005).

Horizontal resolution. The horizontal resolution of a sonar survey is governed by several factors: the sampling density (the number of pings per unit area of the seafloor, which depends on the transmission method, vessel speed and ping rate); the beam footprint, which is determined by the interaction of the sound wave front with the seafloor (how large a part of each ping a feature must occupy to be detected, which depends on the water depth and the wavelength); and the mode of bottom detection (e.g. amplitude, phase).

Modern sonar systems sample the digital returns at rates high enough to represent the signal accurately and therefore sampling should not limit the vertical resolution. However, along-track sampling rates, which are determined by the ship speed and sonar firing rates, can limit the horizontal resolution and detection of targets on the seafloor. The resolution achievable from digital sampling is defined by the Nyquist theorem (Nyquist 1928), which states that a signal can only be resolved if the sampling frequency is at least twice the signal frequency (called the Nyquist frequency). If the sampling density is less than the Nyquist frequency, then the signal will be distorted or even disappear. Signal distortion from under-sampling is called aliasing. The effect of sampling density is easiest to envisage if we consider regular sampling along a sine wave using an SBES in a straight survey line across the seafloor with a field of regular sand waves. The signal in question would, in this case, be the local wavelength and amplitude of the sand waves. In theory, we could reconstruct the sand wave pattern if we had samples of the water depth over each crest and trough (i.e. two samples per wave, the Nyquist frequency). However, we would lose the sand wave signal completely if all our sampling points happened to be exactly midway between each crest and trough. Therefore, in practice, a minimum sampling density of four times the signal frequency is required to overcome the issue of sample locations along the signal. In reality, the spatial frequency of seafloor targets is not known *a priori* and the along-track sampling density is often governed by economic and logistical constraints, so the Nyquist frequency is used only in the interpretation stage to determine the smallest size of object that can be identified in a bathymetric dataset.

The resolution from the wavefront interaction with the seafloor is governed by the first Fresnel zone (Leenhardt 1972; Sheriff 1996) (Fig. 4d). According to Huygen's principle, each part of a wavefront is the source of a new wave and the new wave will start at the same phase that first hit the reflector. New reflected waves will thus form when the acoustic wavefront hits the seafloor. The first Fresnel zone describes the area in which the reflected waves only interfere constructively. Constructive interference occurs when the signals are offset by up to one-quarter of the wavelength. This allows the radius of the first Fresnel zone (R_F) for a vertical sound beam to be calculated by the Pythagorean theorem using the water depth (H) under the transducer and the wavelength (λ), as:

$$R_F^2 + H^2 = \left(H + \frac{\lambda}{4}\right)^2 \tag{14}$$

$$R_F = \sqrt{\frac{\lambda^2}{16} + \frac{H\lambda}{2}}. \tag{15}$$

Because $\lambda^2/16 \ll H\lambda/2$, the expression can be simplified to:

$$R_F \approx \sqrt{\frac{H\lambda}{2}}. \quad (16)$$

Outside the first Fresnel zone, the interference will alternate between constructive and destructive and information is lost. In effect, the echo of a sound pulse that is detected is reflected only from an area with the dimensions of the first Fresnel zone. As an example, a 12 kHz transducer will, at 1500 m s^{-1} sound speed, have a wavelength of 1500 (m s^{-1})/12 000 (Hz) = 0.125 m and the radius of the first Fresnel zone on the seafloor at 1000 m water depth would be *c.* 7.9 m, which implies that objects smaller than this cannot be detected.

Standard acoustic mapping systems

Single-beam echo sounder

An SBES transmits a short sound pulse (typically 0.1–1 ms) vertically down from a transducer with a typically 5–15° wide circular aperture (Lurton 2010). The sound pulse is reflected from the seafloor and is received (usually by the same transducer); the TWT is recorded. Given a knowledge of the water column's sound speed, the TWT is converted to a local depth. Conversions from TWT to depth in the world's oceans were historically made using correction tables developed by D.J. Matthews in 1939. An improved edition of the correction tables was compiled by D.J.T. Carter from the Institute of Oceanographic Sciences, UK in 1980. The latter correction tables were referred to as Carter's tables. Correction tables were used until the 1990s, when measurements of sound speed profiles became a standard procedure in hydrographic surveys. The strength of the returned signal is dependent on the acoustic impedance contrast between the water and the seabed material and can thus also provide information about the type of seabed.

SBESs are typically used as a navigation aid in all types of ship and are by far the most widespread underwater acoustic system. SBESs are usually used in commercial and recreational vessels without motion correction or SVP measurements, except for the surface sound speed, which may be monitored from a seawater intake or estimated by reading the temperature from a sensor and an assumed salinity. Professional SBESs give high-quality depth measurements with accuracies of about 1% of the water depth (Lurton 2010), but their usefulness for mapping glacial landforms nevertheless suffers from their limited spatial coverage and poor horizontal resolution. Despite this, combining SBES data from a large number of ships over long time periods in well-trafficked waters can produce a high sampling density, exemplified by the Olex bathymetric database (e.g. Jakobsson *et al*. 2012). In some areas, especially those traversed regularly by fishing vessels, the accumulated data coverage from Olex is sufficient for the seafloor mapping of features on the order of 10 m in diameter, enabling the interpretation of several types of submarine glacial landforms. Examples of SBES data, acquired by Olex, in submarine glacial landform interpretation have been reported by Graham *et al.* (2008), Clark & Spagnolo (2016) and Ryan *et al.* (2016).

Side-scan sonar

The capabilities, limitations and operational considerations relating to side-scan sonar instruments have been described in textbooks by, for example, Blondel (2009) and Lurton (2010); only a brief summary is provided here. Side-scan sonar systems differ from SBES and multibeam sonar systems because their main purpose is to provide acoustic images of the seafloor rather than measurements of depth. In shallow water, they are usually towed at a short distance from the seafloor in a tow-fish, which makes them relatively insensitive to the ship's motion and noise, while keeping attenuation and spreading losses through the water column to a minimum. Side-scan sonar instruments are usually lightweight enough to be handled manually and can be easily deployed from small boats. Common frequencies for side-scan sonar systems lie in the range 100–500 kHz. Very high frequency side-scan sonar instruments (>1000 kHz) exist for small-target mapping as well as low-frequency systems (<10 kHz) for deep water applications (Somers *et al.* 1978). Side-scan sonar systems are used predominantly in shallow water because the lower frequency systems are large and MBESs with backscatter capabilities are now becoming standard on research vessels.

The working principle of a side-scan sonar system is simple: it sends out two sound beams that are as wide as possible across-track and as narrow as possible along-track (horizontal width usually <1°) at oblique angles to each side of the tow-fish. The sound beams intersect the seafloor along a thin strip and use a very short pulse that spreads outward with time, allowing the detection of small objects. A high-frequency (>500 kHz) side-scan sonar is, in theory, capable of mapping centimetre-scale objects. The echoes received record a time series of backscatter, and especially irregularities in the topography, of the seafloor along the swath. Each recorded reflectivity swath is geo-referenced and added to the previous swath; an image of the seafloor can therefore be generated by colour coding or grey shading the backscatter values. A major advantage of the side-scan sonar technique is the low incidence angle, which makes the sound beam cast shadows away from the tow-fish behind even small topographic features. The length of such shadows can, together with the incidence angle (based on the distance from the nadir), be used to estimate feature height. Because the side-scan sonar instrument uses two transducers directed away from each other, there will always be a narrow strip of the seafloor directly below the tow-fish (at the nadir) with no data. This strip will become wider as the distance of the tow-fish from the seafloor increases, but may be edited away at the interpretation stage to produce more accurate and better-looking mosaics. The integrated arrivals at both sides and closest to the central strip with no data also provide an indication of the bathymetric profile along-course. In practice, one of the most crucial aspects of side-scan sonar surveying is keeping the height of the tow-fish over the seafloor constant, as this may otherwise lead to distorted records requiring correction. Modern side-scan sonar systems are able to operate at more than one frequency so that they can better resolve objects and structures of different sizes.

The resolution of a side-scan sonar system is difficult to quantify because it is inhomogeneous and varies along the ensonified swath both along- and across-track. If not compensated for, this results in elongated pixels with varying aspect ratios along each swath. However, modern side-scan sonar systems use electronic phase-steering of the transducer elements in the array to focus the received signals from each part of the swath (Wille 2005). Heading variations in the tow-fish will turn the swath horizontally, causing geometrical problems. For the highest possible accuracy, these can be compensated for using ancillary navigation and motion-control devices.

Depth measurements are possible with interferometric side-scan sonar systems, also known as phase-differencing bathymetric sonar systems, by using one or more additional receiver arrays mounted in parallel to the main array. The phase difference between the signals received on the additional arrays (set a known distance apart) is used, together with the roll angle of the tow-fish, to calculate water depth. This method yields an extremely high data density, but often suffers from being very sensitive to noise and the potential for the miss-picking of phase cycles; the bathymetry data derived from MBES is still usually superior in all aspects, except for the fact that a very wide swath can be achieved with a side-scan instrument (Lurton 2010).

Multibeam echo sounder

An MBES involves the same fundamental echo-sounding principle as an SBES; most of the seafloor images in this *Atlas* were acquired using these systems. The travel time of a transmitted sound wave reflected back from the seafloor is converted to water depth by applying the speed of sound in the water column (i.e. the SVP). The geometry of the transmitted sound waves, however, resembles more that of a side-scan sonar system than an SBES. Viewed from the across-track direction, the MBES transmits sound waves in a wide fan (Fig. 5). The full width of the fan, commonly referred to as the swath width, is measured as the angle α between the outermost port and starboard sound waves to the -3 dB sound level (Fig. 5). Modern conventional MBESs typically have a value of α of the order of 130–150°. The receiving transducer array is rotated 90° with respect to the transmitting array in a configuration called a Mills cross or Mills T (Fig. 5). Although the transmitting swath is made as wide as possible in the across-track direction, it is made as narrow as possible in the along-track (fore–aft) direction. By contrast, the receiving array is optimized to form multiple receive beams that are as narrow as possible in the across-track direction – a process called beam-forming. This configuration results in a receive footprint on the seafloor that is the intersection (cross-product) of the narrow along-track transmitted beam and the narrow across-track received beam. Each of these narrow beam footprints represents an individual high-resolution depth measurement across the full swath (Fig. 5). Some modern MBES systems can use phase detection techniques within the beam footprint to extract multiple depth solutions (in the across-track direction) within the intersection of the transmit and receive beams. The end result from a single MBES ping is a swath of seafloor depths at the highest possible resolution. The width of the strips – that is, the beam width for modern MBESs – is typically between 5 and 0.5°.

From equation (12) it is clear that the resolution of a specific MBES is influenced by the frequency and length of the transducer array. Higher frequency and longer transducer arrays will result in narrower beam widths and smaller footprints on the seafloor.

The transmitted sound waves are traced geometrically through the water column based on a knowledge of the SVP and detailed measurements of the motion of the vessel (heave, pitch, roll and yaw; Fig. 5) during each transmit and receive cycle. Resolving this rapidly changing geometry provides one of the main challenges in determining an accurate representation of seafloor depths. Non-vertically transmitted sound waves will refract during propagation through the water column when there is a sound speed gradient in the water column. This implies that an accurate SVP is required for the surveyed area. In addition, from a geometrical perspective, the accuracy of the depth measurements is also highly dependent on the accurate measurement and compensation of the effects of the ship's motion as well as the time latencies with respect to the transmit and receive signals (Fig. 5).

Given the long lever arms (i.e. the long distance between the transducers and the seafloor depths provided by the outermost beams) associated with wide swath widths, problems with MBES data with inadequate motion compensation and inaccurate sound speed corrections often manifest as a degradation in the quality of the data, particularly for the outer beams. To minimize this, MBES systems can cut returns from the outer beams, especially in unfavourable sea conditions, which leads to a narrower coverage per swath. In addition, the geometry of the swath produces a higher resolution (i.e. smaller footprint) in the less oblique central beams and a lower resolution (i.e. larger footprint) in the more oblique outer beams. There are different approaches to minimizing these effects, such as using the MBES system in the so-called equal-beam spacing mode, or narrowing the full swath width so that there is a higher density of data across-track, but the fundamental geometry of narrower beam footprints near the nadir remains the same.

In addition to the instantaneous measurements made by echo sounders to determine depth (both by SBESs and MBESs), the

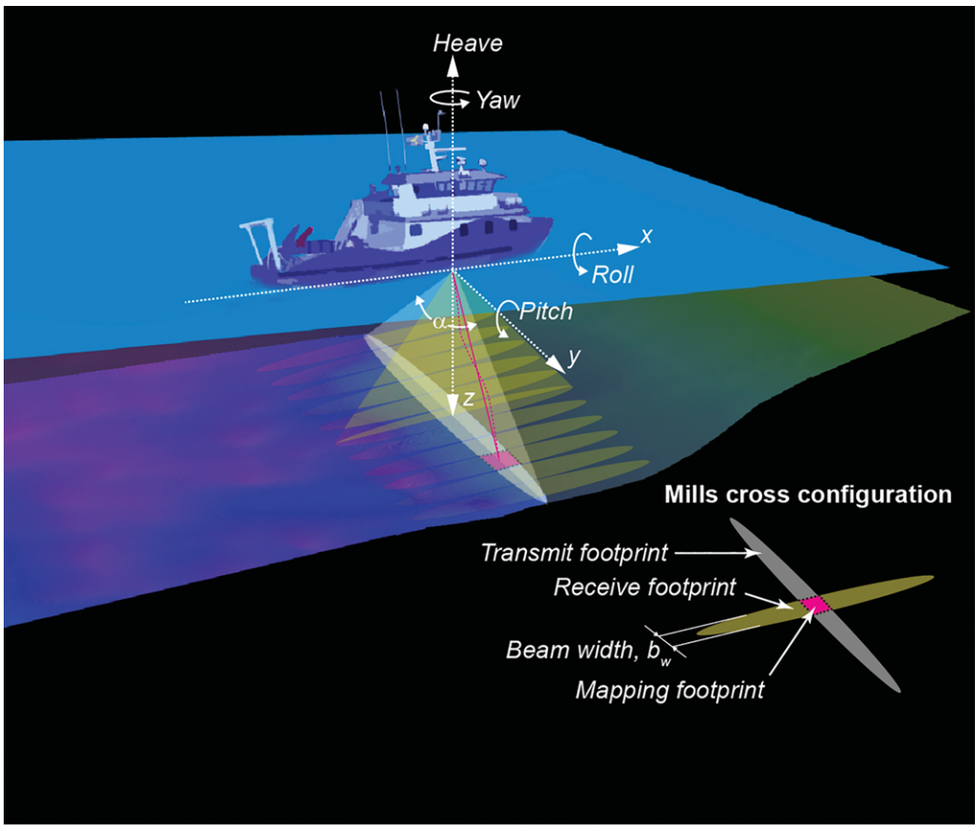

Fig. 5. Schematic illustration of an MBES system and the ship's motions that need to be accounted for to acquire high-quality multibeam swath bathymetry.

amplitude of the returned sound can be recorded to offer some insight into the nature of the seafloor (referred to as reflectivity for SBESs and acoustic backscatter for MBESs and side-scan sonar systems). Side-scan sonar offers a measurement of backscatter from the seafloor, but without any angular information about the return (i.e. a flat seafloor is assumed) and the backscatter from both MBESs and side-scan sonar systems can be used to construct geo-located backscatter images and compiled mosaics that can be useful for viewing the geometry of seafloor features and identifying changes in the nature of the seafloor properties. Early systems were rarely (if ever) calibrated, so backscatter or reflectivity measurements were relative measurements that could be used to interpret major changes in seafloor type (assuming the instrumental settings remained constant), typically based on the relative amplitude of the return (for reflectivity) and the relative amplitude and image texture of backscatter. Backscatter from MBESs offers the opportunity to look at the angular dependence of backscatter as a possible indicator of seafloor type (Fonseca & Mayer 2007) and, with the latest generation of broadband MBESs, there is now the opportunity to look at the frequency dependence of backscatter to provide an additional tool for seafloor characterization (Hughes Clarke 2015).

Sub-bottom profilers

Sub-bottom profilers (SBPs), also known as sediment profilers, are echo sounders designed to penetrate the seafloor and measure the travel time (depth) to layers in the uppermost sediments. They operate on the same principle as SBESs, but with higher output energy levels and lower frequencies, which allow penetration into sedimentary material below the seafloor. The downward signal is reflected, in part, at any boundary with a strong enough impedance contrast and the pulse continues down until all of its energy has been absorbed. The variations in amplitude with travel time of the recorded reflections are colour coded (usually grey shaded) and successive pings are stacked to form a profile image of the reflections within the sediments. The impedance contrast, reflectivity and absorption coefficient of the target sediments can be estimated and visualized in some SBP systems, which increases the interpretation possibilities.

SBPs usually operate with frequencies in the range 1–20 kHz and penetrate up to about 100 m in soft, low-absorbing sediments, but commonly only several tens of metres in many environments. Penetration >10 m in soft sediments may be achieved occasionally with frequencies >20 kHz in relatively shallow water (<100 m water depth). The simplest SBP systems are the fixed-frequency (CW) SBPs (known as pingers), which commonly operate at 3.5 kHz.

The horizontal and vertical resolutions of an SBP with a fixed frequency are calculated in the same way as for an SBES. The vertical resolution of an SBP will increase at higher frequencies, but the penetration increases at lower frequencies (see the earlier sections on resolution), which results in a trade-off. Various techniques have been developed to increase the penetration while keeping the resolution as high as possible, such as the chirp sonar (FM) and the parametric echo sounder.

SBPs are designed to use only reflected echoes, unlike acoustic methods aiming to map the seafloor surface where the backscatter component is also utilized. This has important implications for interpretation, as described further by Lurton (2010):

- A sub-bottom profiler gives the best results when the incidence angle of the transmitted wave is near-vertical to the seafloor. The direct echo of a reflected low-frequency signal is then much stronger than the backscattered echoes. At oblique angles, the reflected signal will be diverted away from the sensor and only very weak, backscattered echoes will be detected, which will most often be obscured by noise.
- The resulting quality of an SBP profile is highly dependent on the signal's wavelength, but is, in principle, independent of the beam width for a flat seafloor. However, a broad beam is more likely to produce side echoes and hyperbolas if small targets are present (see sections on artefacts for further discussion).
- The profile quality is relatively insensitive to roll variations in the vessel, as long as the main lobe of the sound pulse contains the direction of the specular reflection.

The horizontal resolution of an SBP is governed primarily by the first Fresnel zone and not the footprint (see section on horizontal resolution) because the method is based on recording the direct reflection and not the backscatter (Lurton 2010). The vertical resolution of a fixed-frequency conventional SBP (pinger) is governed by the Rayleigh criterion (see section on vertical resolution, equation 13).

Chirp sonar

Chirp sonar is a common type of SBP system capable of producing higher quality profiles than conventional SBPs. Instead of using a fixed frequency, a chirp sonar transmits an FM pulse that sweeps through a frequency range of several kilohertz. The sound of the generated pulse sweep, usually from low to high frequency, resembles a bird's chirp – hence the name chirp sonar. The frequency range commonly lies somewhere between about 500 Hz and 24 kHz. The pulse lengths of chirp sonars are commonly 10–50 ms – that is, up to hundreds of times longer than for conventional SBESs, which allows much more energy to be transmitted in each pulse. The FM pulse is compressed using matched filtering (Schock *et al.* 1989), which means that the returning chirp signal is correlated in the time domain with a stored copy of the outgoing pulse; this collapses the pulse to a short duration wavelet (Fig. 6). From an originally long-duration pulse with a relatively low peak amplitude, a chirp pulse after matched filter compression is capable of producing a narrow pulse with a high peak amplitude, which is required to maximize the penetration and resolution. The length of the pulse allows a substantial amount of energy to

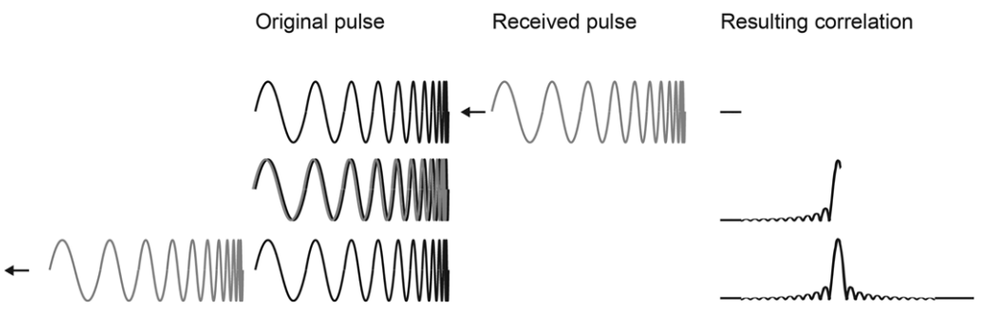

Fig. 6. Schematic conceptual visualization of matched-filter correlation of a chirp sonar signal. The envelope of the autocorrelation function of the signal gives a strong central peak and suppression of noise. (1) In principle, the received signal is slid past a replica of the transmitted pulse (by shifting the time) and the corresponding correlation is calculated at each step. (2) Maximum correlation (central peak) occurs when the signals overlap completely. (3) The autocorrelation function is complete when the signals have passed each other entirely.

be transmitted. Because noise does not correlate with the filter, a high SNR is obtained.

The vertical resolution R_v (m) of a chirp sonar system may be estimated by:

$$R_v = \frac{v}{B/2} \quad (17)$$

where v is the sound velocity and B is the bandwidth – that is, the difference between the highest and lowest frequency limits of the signal used.

Parametric echo sounders

The compressibility of water is non-linear, which means that the peaks of pressure waves (such as sound pulses) will travel slightly faster than the troughs. This will distort the pulse during its propagation from its original sinusoidal shape to a more saw-toothed appearance. This effect is smaller than the ambient noise and absorption effect in conventional echo sounders and does not affect the sonar performance to any great degree. However, the non-linearity parameter of water is utilized in so-called parametric echo sounders. A saw-toothed waveform consists of additional frequencies (higher harmonics or overtones), as opposed to the pure tone of a sine wave. This very weak effect is utilized in the parametric echo sounder by transmitting sound with a high intensity at two frequencies (separated by the desired frequency value) simultaneously from the transducer. The interference of these two signals will, as a result of non-linear mixing, generate secondary frequencies where one is equal to the sum and another is equal to the difference between the original frequencies. The summed secondary frequency will be very high and is quickly attenuated, whereas the difference frequency will be low and propagate further. This secondary frequency will occur only at the highest energy levels in the central part of the beam, which creates a very narrow, low-frequency beam with virtually no side lobes (Mosher & Simpkin 1999; Lurton 2010) without the need for a long transducer array. The non-linear mixing is only possible during transmission because the weak interference effect requires a high intensity sound, whereas the echoes will be relatively weak. The receiving in parametric echo sounding is therefore conventional (the same as for an SBES), with a wide beam. The narrow transmit beam offers better horizontal resolution, but requires compensation for the ship's motion to be useful.

The penetration and vertical resolution achievable with parametric echo sounders are comparable with those of chirp sonars. The vertical resolution can be estimated as for a chirp sonar system (equation 17) because the bandwidth is close to 100% of the secondary frequency. The narrow beam width of parametric echo sounders is foremost an advantage when surveying small (lateral extent) features not expected to form specular reflections – for example, for fine-scale objects such as buried pipelines, dropstones or narrow channels.

Seismic-reflection profiling

There is a wealth of literature describing the seismic-reflection method for mapping sub-bottom geology because the technique has formed the backbone of the hydrocarbon exploration industry for several decades (e.g. Sheriff & Geldart 1995; Ashcroft 2011). Only a brief overview of the fundamentals is therefore provided here.

There are two main types of seismic-reflection mapping: 2D seismic and 3D seismic. The former acquires sub-bottom information along 2D profiles, whereas the latter acquires 3D data in a regular and closely-spaced grid. A fully imaged 3D cube, extending from the seafloor to the base of the acoustic penetration, is derived from a 3D seismic-reflection survey, whereas a 2D survey produces a set of interpretable individual sub-bottom profiles.

The acoustic principle of the seismic-reflection method is the same as for SBP, although the source and receiver are always separated (Fig. 3). The source is commonly towed relatively close to the ship, whereas the receiver consists of a long towed streamer with many piezoelectric elements referred to as hydrophones. These hydrophones are either connected together to constitute one receiving channel or in groups to produce several channels, usually 24, 48, 96 or more channels. A single-channel streamer is typically tens of metres in length, whereas a multi-channel streamer can be of the order of hundreds of metres to kilometres in length. The single-channel set-up is thus considerably smaller and cheaper to operate and is often used on research vessels to complement a hull-mounted SBP system with deeper sub-bottom penetration. Although there is an advantage in the compactness of a single-channel seismic-reflection system, the potential for enhancement during signal post-processing is considerably less than for a multi-channel system, which also has the advantage of providing information on the seismic velocities of layers below the seafloor. The geometry between the source and a suite of separated receiving channels can be used to improve the SNR as well as to remove artefacts that may otherwise obscure geological interpretation. A particular advantage of multi-channel data in continental shelf environments is that the range of source–receiver offsets can be used to suppress seafloor multiple reflections. Signal processing of seismic-reflection data is the subject of many books (e.g. Upadhyay 2004; Zhou 2014), software suites and has a research field of its own.

The most common seismic sources used in marine seismic-reflection surveys displace water rapidly to produce a pressure pulse in the form of a sound wave. So-called boomers (Edgerton & Hayward 1964) and air and sleeve guns (Parkes & Hatton 1986) belong to this category. The former generate a pressure pulse driving one or more copper or aluminium plates rapidly apart from one or more flat spiral coils in the water. This is achieved by discharging electricity through the flat spiral coil, which induces electrical currents opposite to the coil current that drive the coil and the nearby mounted plate apart. The plate flexes in the water and produces a pressure pulse. The boomer source is capable of producing a clean pulse, generally in the frequency range 0.5–1.5 kHz, although the bandwidth of the source signature may extend to as much as 20 kHz (Simpkin 2005). It is therefore close to a low-frequency SBP in performance with respect to resolution, but often gives superior penetration.

Air gun and sleeve gun sources are based on releasing high-pressure air into the water. They are capable of generating substantially lower frequency pulses than a boomer, extending to <10 Hz and with peak frequencies typically in the range 20–100 Hz, resulting in much deeper sub-bottom penetration at the expense of resolution. The volume of the air chamber is correlated broadly with the frequency of the source signature and the peak output pressure power (measured in bar). An air or sleeve gun with a large chamber is capable of generating a lower frequency pulse with a higher peak output pressure than one with a small chamber. Air and sleeve gun chambers range in size from <0.3 to >10 l. An intermediate-sized air gun with a 0.7 l chamber is capable of providing signal penetration >1000 m beneath the seafloor under favourable conditions.

In contrast with the seismic sources described earlier, which all produce a positive pressure pulse, the so-called sparker uses the collapse of a bubble (implosion) to produce its outgoing pulse (Edelmann 1968). A high-voltage electrical charge is released from capacitors across open-ended electrodes so that a 'spark' is created in the water. This spark produces an expanding and collapsing high-pressure vapour bubble. The typical frequency range of sparkers is between 20 and 200 Hz.

Towed seismic sources generally produce high-energy pulses with frequencies between 10 and 4000 Hz, implying that they will penetrate deeper into the sub-bottom than most common SBP systems and are therefore also capable of imaging the

sub-bottom geology to significant depths. The airgun sources are at the lower end of the frequency range, whereas boomer and sparker sources are at the higher end. A further discussion of high-resolution marine seismic-reflection sources and their characteristics can be found in Mosher & Simpkin (1999).

The depth at which seismic sources and receivers are towed modulates the frequency content of the recorded signals and thus affects the resolution of the data. This is an effect of interference with reflections from the sea surface, which suppresses the frequencies for which the towing depth equals half a wavelength and reinforces the signals at half that frequency. As an example, for a sound speed of 1500 m s^{-1}, a towing depth of 2.5 m results in the suppression of frequencies around 300 Hz and the maximum reinforcement of frequencies around 150 Hz. The acquisition of good quality high-resolution seismic data requires towing the source and receivers at a relatively shallow depth. In adverse weather conditions or waters covered with sea ice, however, it is often necessary to increase the depth at which hydrophone streamers are towed to reduce swell noise or avoid sea ice in the ship's wake, thus compromising on resolution.

3D seismic data

Early 3D seismic-reflection datasets were collected by vessels towing a single hydrophone streamer along a set of parallel lines spaced only a few tens of metres apart (e.g. Shipley *et al.* 1992). The towing of multiple streamers, with paravanes used to maintain tens of metres of separation between them, became increasingly common during the 1980s, greatly increasing the efficiency of 3D data collection. Many modern commercial seismic vessels are capable of towing up to 12 streamers many kilometres in length and some can tow an even larger number (Fig. 7). Multiple airgun arrays are also commonly used to increase the spread of reflection points on and below the seafloor. Even when using multiple streamers and airgun arrays, however, the collection of commercial 3D seismic data requires a specialized vessel to work in a relatively small area over many days or weeks and is thus a costly enterprise. The high quality of the data and the additional options they provide for the detailed analysis of subseafloor structures and stratigraphy make the collection of 3D data a worthwhile investment for oil and gas exploration companies over wide areas considered to be prospective and especially over proven fields. It is not uncommon for 3D surveys over producing fields to be repeated to monitor the effects of hydrocarbon extraction on the reservoir; such time-lapse imaging is referred to as 4D seismic.

3D seismic data enable enhanced processing and a wide range of additional interpretation approaches compared with 2D data. The precise positions of the airgun arrays and streamers are monitored by a range of navigation tools, including global positioning system (GPS) receivers on floating structures such as tail buoys, acoustic transponders and compass sections within the streamers. The locations of reflection points for each source–receiver pair are calculated and the recorded data are gathered into a regular grid of bins that are each just a few metres across. The continuous 3D grid of data points allows seismic migration algorithms to be applied in three dimensions, which enhances imaging by correctly repositioning the reflected arrivals along hyperbolae to their true source points. By contrast, the migration of hyperbolae from linear structures in 2D data only works correctly if the structures are

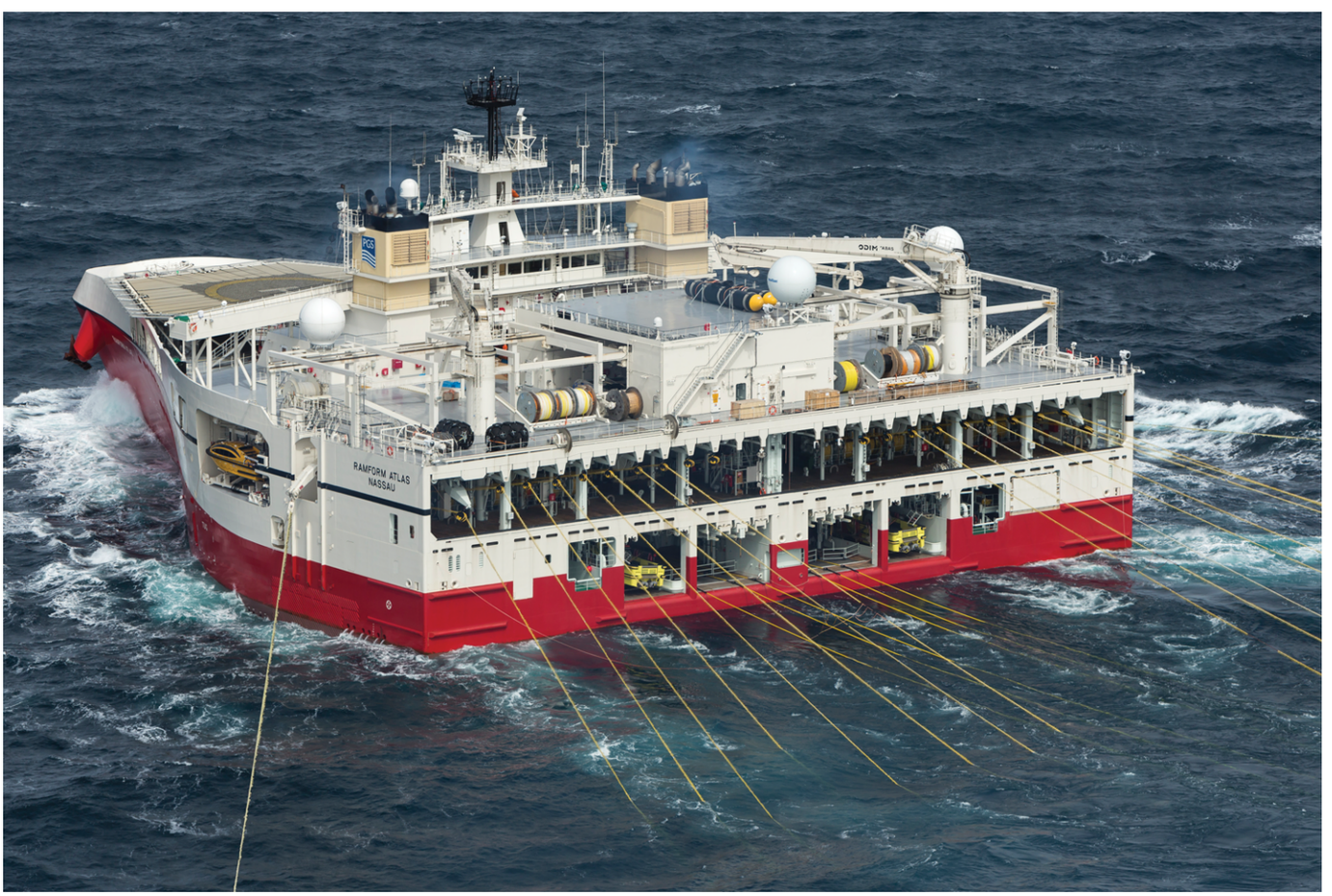

Fig. 7. The 104.2 m long and 70 m wide 3D seismic survey vessel *Ramform Atlas,* part of the fleet of the marine geophysical company PGS. This vessel belongs to their Titan class and is equipped with 24 streamer reels. Photograph courtesy of PGS.

nearly perpendicular to the line or if unrealistic seismic velocities are provided as input.

Processed 3D data cubes can be inspected and visualized in a range of ways that provide detailed images and information on the properties of material below the seafloor. In addition to conventional profiles along each line, cross-profiles in any orientation can be extracted from a 3D cube. 3D cubes can also be cut horizontally to produce maps of reflected amplitudes on time slices at any specified two-way time. A further way to visualize data within a 3D cube that can provide better images of specific features is to extract maps of reflected amplitudes at the seafloor and other specific interpreted horizons. This requires additional work in that it is necessary to pick the horizons first. 3D software interpretation packages include automated picking tools that can help with this task, although their picks usually need to be guided and checked by a skilled human interpreter. Such analyses can reveal the geometry of specific features of depositional systems such as channels. In data from past glacial environments, investigations of 3D cubes can image features such as tunnel valleys, iceberg ploughmarks and subglacial bedforms on buried palaeosurfaces (e.g. Andreassen *et al.* 2004, 2007; Dowdeswell & Ottesen 2013; Stewart *et al.* 2013).

A high-resolution 3D seismic system that has been utilized widely for more than a decade in different geological settings is P-Cable, which we use as an example of this increasingly common and commercially available method. This system has a specific potential for mapping submarine glacial landforms as a result of the high resolution achievable and the compact nature of the equipment, which means that it can be deployed from many multipurpose research ships.

The P-Cable is a lightweight 3D seismic system consisting of a cross-cable that is towed perpendicular to the ship's steaming course, two side paravanes, streamers and ancillary components (Fig. 8). The two paravanes, one at each end of the cross-cable, keep it extended. The geometry of the system is variable. It may include 12 or more 25–100 m long streamers that are attached by one end to the cross-wire at intervals of several metres and are towed behind the vessel. The cross-cable powers up to 24 active sections and also ensures communication with the vessel control unit. The towing depth of the cross-cable with the streamers is usually from 1 to 3 m. Two tow ropes and signal cables, one per side, complete the system's configuration (Fig. 8). The source and its deployment are generally standard (e.g. four 0.6 l airguns or a 3.4 l generator-injector airgun) towed behind the vessel's stern. The positioning of the seismic array is performed using GPS (with full real-time kinematic or differential correction) with two antennae on the paravanes, one on the gun's float and one onboard. This configuration allows the imaging of a swath of the sub-bottom up to 150 m wide on each collection line at water depths ranging from 300 m to more than 3000 m (Planke *et al.* 2009*a*, *b*).

The product obtained after combining the data for each collection line is a high trace-density seismic 3D cube usually covering an area of 10–50 km^2 at high resolution (50–250 Hz), which typically requires three to five days of ship-time to be acquired (Planke *et al.* 2009*a*). The effective vertical and spatial resolution are improved when a high-frequency seismic source is utilized. The data are frequency filtered (e.g. 45–220 Hz) and binned before migration. The use of small offsets and a close streamer spacing leads to dense, common mid-point coverage with bin sizes as small as 6×6 or 3×3 m in the latest developments (http://pcable.com/). Both the vertical and horizontal resolution are therefore much finer than in conventional 3D seismic surveys.

P-Cable has been applied on Arctic and sub-Arctic margins, where it has imaged, in great detail, the configuration of buried

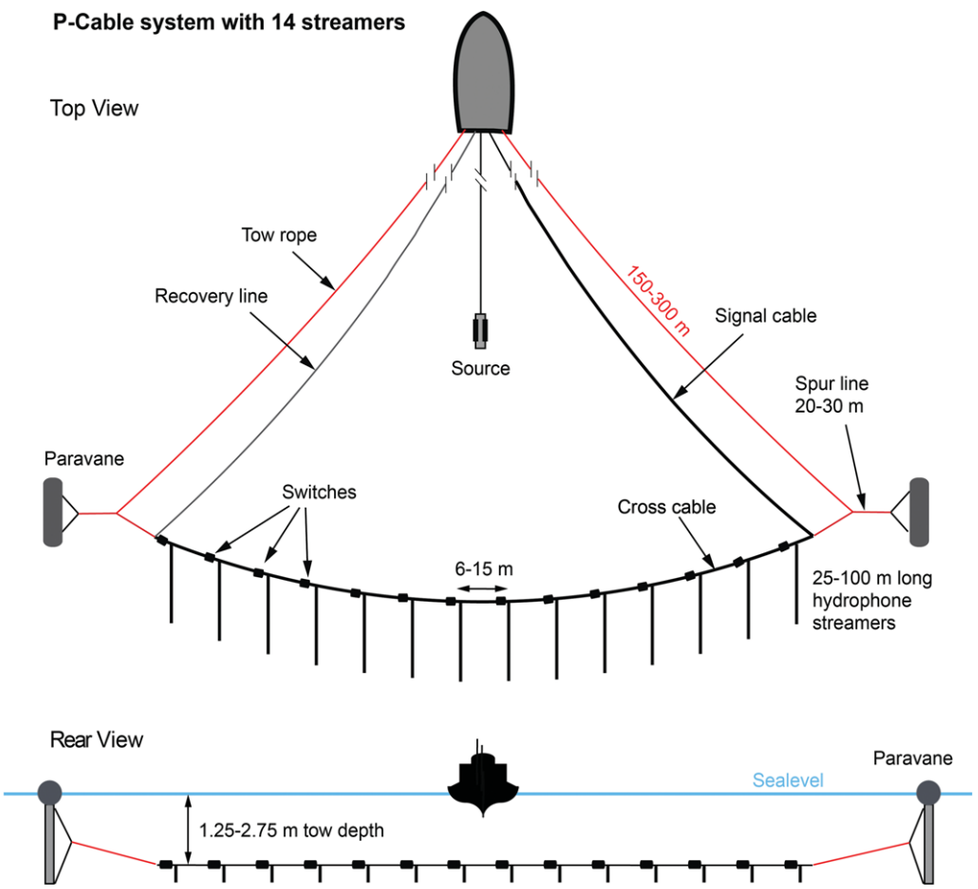

Fig. 8. Schematic illustration of the patented P-Cable 3D seismic data acquisition set-up. Illustration is based on drawing provided by P-Cable (www.pcable.com)

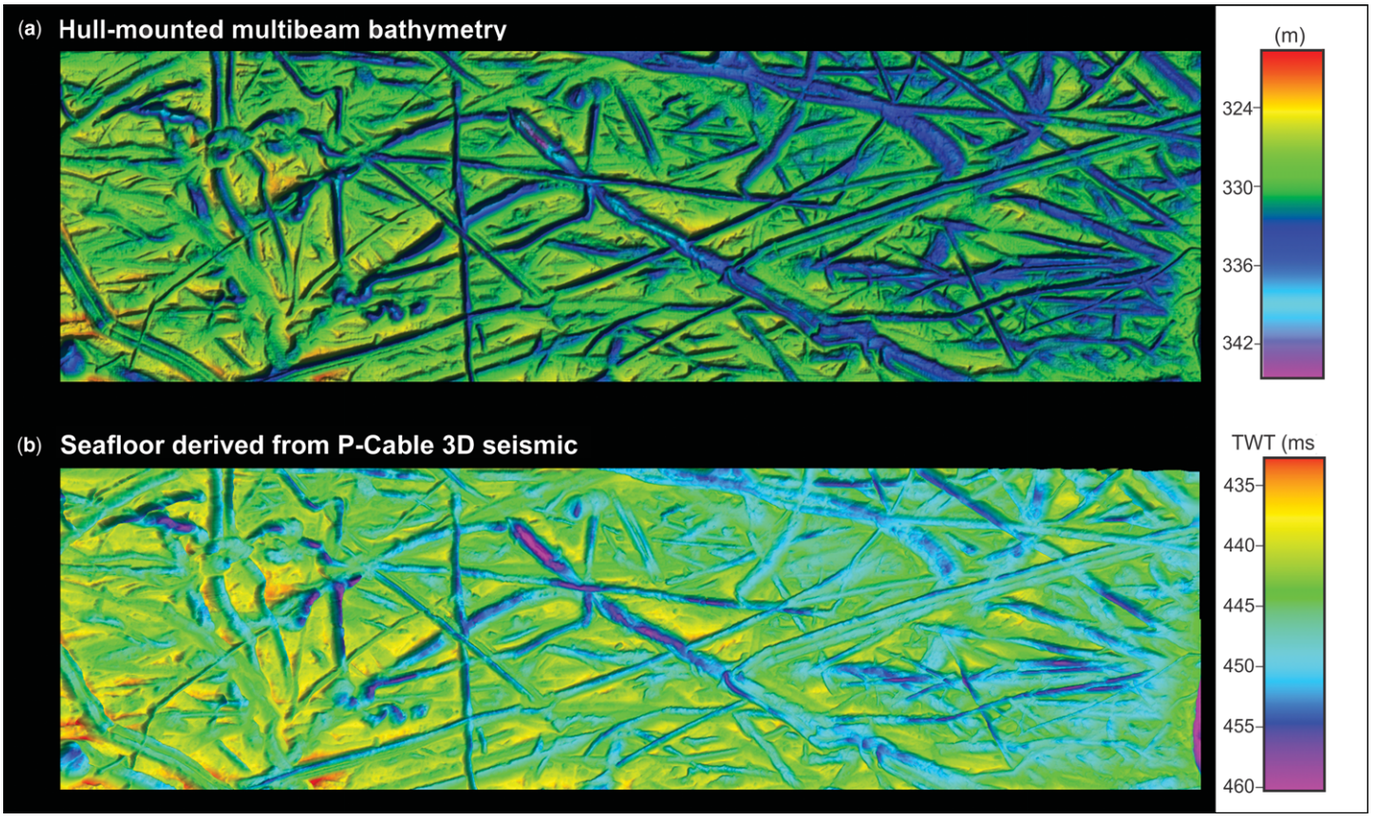

Fig. 9. Comparison between seafloor bathymetry derived from a P-Cable 3D seismic survey (**b**) and multibeam bathymetry (**a**) in an area dominated by iceberg plough marks. Figure courtesy of Stefan Buenz, UiT, the Arctic University of Norway.

iceberg ploughmarks, streamlined glacial landforms and many other features, such as gullies, erosional surfaces and unconformities, landslides, fluid leakage pathways, shallow gas, gas chimneys, hydrate-bearing sediments, pockmarks and mud volcanoes (e.g. Bünz *et al.* 2005, 2012; Petersen *et al.* 2010; Perez-Garcia *et al.* 2011; Berndt *et al.* 2012; Lafuerza *et al.* 2012; Brookshire *et al.* 2015).

The horizontal resolution of P-Cable compares well with state of the art multibeam systems and is even superior to most hull-mounted MBES systems used for deep water studies (Fig. 9). In addition, because of its sub-bottom penetrating capability, an advantage of P-Cable and similar systems used in academia and industry is that amplitude information is easily obtained and represents a powerful piece of information for interpretation purposes, allowing the estimation of changes in the sub-seafloor acoustic impedance. However, the cost of the acquisition and processing of 3D seismic data far exceeds that for multibeam sonar. Furthermore, 3D data acquisition requires the deployment and recovery of a large amount of towed equipment, making it impracticable in areas with sea ice, and the rate of data acquisition is limited by the towing speed of 5 knots. The short streamer lengths used in the P-Cable system limit the processing options for the suppression of multiple reflections from the seafloor. Consequently, its main applications are at relatively shallow sub-seafloor depths, but this is not a major limitation for studies of most glacial depositional systems.

Errors and artefacts

Artefacts in geophysical mapping data derived from acoustic methods are defined here as false features that appear from acoustic, geometric or processing phenomena and therefore do not represent the real seafloor, sub-bottom morphology or geology. An artefact may, in the worst case, directly mislead the scientist interpreting the acoustic mapping results. It should be pointed out that all acoustic images derived from geophysical mapping are merely portrayals of the geology assembled from sound reflections. A classic example of an artefact is multiple reflections of the seafloor and/or sub-bottom geological boundaries that appear in sub-bottom and seismic-reflection profiles. Multiples are further described, along with illustrative examples, in the section treating the most common artefacts in sub-bottom and seismic-reflection profiles.

Some artefacts are the result of the acoustic noise sources common to all acoustic systems. Sources of acoustic noise include ambient noise that is not derived from the sonar system but rather from natural (e.g. rain, wave action, biological) or human-derived (e.g. shipping) sources, the internal noise of the instrument system (e.g. electronic), reverberation and interference. These noise sources can have a wide variety of impacts on the received acoustic signals that are difficult, if not impossible, to catalogue. A detailed discussion of these forms of underwater acoustic noise is found in Lurton (2010).

We focus here on describing the most common artefacts that may obscure or degrade the glacial landform record potentially revealed in geophysical mapping data. The discussion is based on real examples with the goal of providing a look-up table for some of the most commonly appearing artefacts. There is a bias towards examples from MBES results because this is the most widely used method for studies of submarine glacial landforms today and the main focus of this *Atlas* is on such images. Artefacts in MBES data were pointed out at an early stage as a problem for scientists interpreting multibeam images, especially when they do not have full insight into the engineering of the sonar systems (de Moustier & Kleinrock 1986).

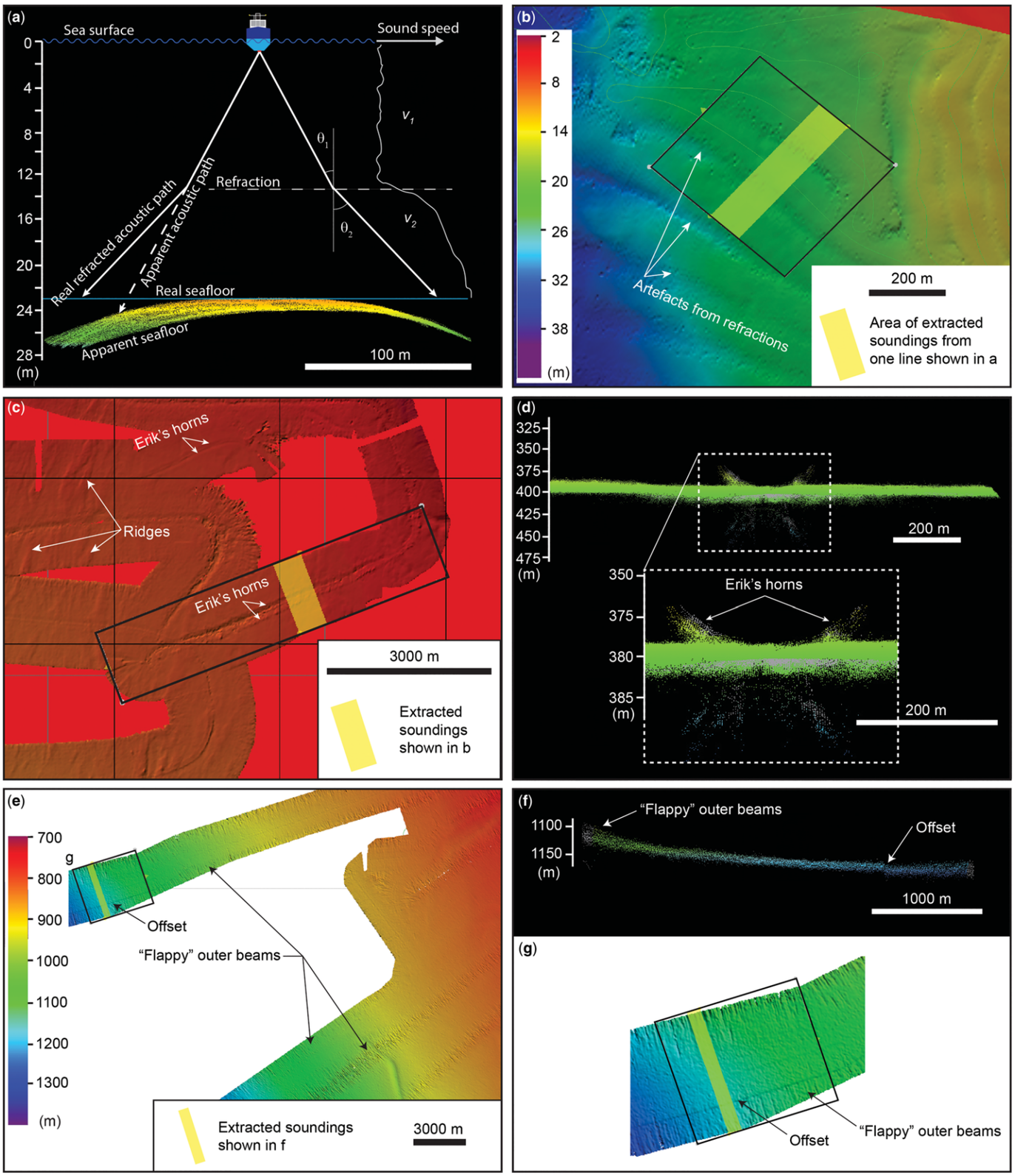

Fig. 10. Common artefacts encountered in multibeam mapping. (**a**) Schematic illustration showing the problem of refractions caused by poor sound speed control. (**b**) Multibeam swath bathymetry with clearly visible artefacts from refractions due to poor sound speed control. In this case, the outer beams are bent downward, as illustrated in (a). This results in a false trench where overlapping swaths from adjacent survey lines meet. (**c, d**) Multibeam swath bathymetry with accentuated Erik's horns. The profile in (d) is viewed from the rear and shows individual soundings (see text for discussion). (**e**–**g**) Irregular and noisy, 'flappy' or 'wobbly' outer beams and prominent bathymetric offsets across-track. Flappy outer beams are commonly accentuated by poor sound speed control, whereas distinct offsets may be problems related to signal processing and bottom detection algorithms. All multibeam examples shown were acquired by the Swedish icebreaker *Oden*. Acquisition system Kongsberg EM 122. Frequency 12 kHz.

MBES

Refractions. Refractions of a sound wave propagating through the water column will naturally occur according to Snell's law where the wave encounters an acoustic impedance contrast (equation 2; Fig. 4a). In reality, changes in acoustic impedance in the water column are usually gradational, resulting in gently curved ray paths. This must be corrected for by tracing the acoustic wave through the water column and adjusting it back to a straight path in all calculations. A method commonly referred to as ray-tracing is applied, with the specific algorithms used for this method varying slightly between applications. A knowledge of sound speed variations through the water column is required to perform this correction, which is provided through acquiring SVPs during data acquisition in multibeam surveys. The refraction phenomenon is most commonly manifested through the entire swath of across-track data being bent upwards (smiling) or downwards (frowning) towards the outer beams (Fig. 10a). It may be difficult to identify in complex seafloor topography or along a single track, but in a survey with overlapping swaths it is easily detected because the depths of the outer beams in overlapping swaths will not match properly, causing the surveyed area to have a striped appearance (Fig. 10b). An effective way to avoid this problem is to acquire sound speed profiles regularly in the survey area or, even better, to tow an underway sound speed profiler capable of collecting data throughout the entire survey. However, if high-quality SVPs have not been collected, there are post-processing approaches that will suppress at least the most striking refraction artefacts. These approaches use a flat part of the surveyed area to calculate refraction coefficients that can then be applied across the survey to remove the anomalies.

Erik's horns. Prominent ridges appearing along the survey track on either side of nadir are often referred to as Erik's horns (Fig. 10c, d). The nickname of this artefact originates from the time it was first recognized during the development of the EM1000 MBES by Erik Hammarstad and Freddy Pohner. They described the horns in the documentation for the Kongsberg echo sounder and ascribed the cause of the problem to the difference in bottom detection location when the bottom tracker switched from selecting the bottom based on the centre of mass of the return in the footprint (amplitude detection) to the centre of the beam as selected by the zero-phase difference between two virtual beams created within the beam footprint (phase detection). Amplitude detection typically takes place near the nadir (or on inward-facing slopes) where the time series of the return is too short to undertake robust phase detection. As soon as the time series is long enough to undertake phase detection, this method is preferred. The original cause of Erik's horns appears to have been resolved in newer MBES instruments; however, a similar artefact is now often found and is probably related to the development of bottom detection algorithms that account for sub-bottom penetration on soft seabeds (Fig. 10c, d). Erik's horns are among the more difficult artefacts to remove in post-processing. Such artefacts are more noticeable in areas of relatively flat seafloor.

Wobbly outer beams and offsets. The final depth values produced by MBES systems are a result of the integration of a number of components including the sonar, the sound speed sensor, the motion sensor, the navigational system and a time base. An accurate knowledge of the relative alignment of all these sensors, as well as an accurate record of their movements during transmit and receive cycles, is crucial in obtaining high-quality depth information. Misalignments or an improper understanding of the true alignments or other integration parameters can lead to a number of subtle artefacts in the resulting bathymetry that manifest themselves as ribbing, typically across the swath profile. Such artefacts are often fairly small and subtle, but they can become prominent with modern 3D data visualization techniques using artificial sun illumination and may lead to misinterpretations of the data.

To address the issue of sensor misalignments, MBES-equipped vessels should undertake a patch test, which attempts to determine the consistency of the sonar when surveying over a patch of the seafloor with known features under differing survey conditions – for example, steaming back and forth in opposite directions over a flat area of seafloor to check for roll biases or steaming over a slope at different speeds to check for time latencies or pitch biases. Correction coefficients are inferred for any biases that are determined, either directly in the MBES acquisition software or during post-processing. A patch test can also resolve relatively static misalignments between the sonar and the roll, pitch and heading sensors as well as time latencies between the sonar and the navigation system.

The patch test examines relative offsets between the sensors, but not necessarily the alignment of the sensors with respect to the ship's coordinate frame. If there are errors in the alignment of the sensors with respect to the ship's reference frame as well as uncertainty in the spatial and temporal variability of the sound speed profile, other dynamic errors can result that also manifest themselves as ribbing across the swath and are commonly referred to as wobbles. Hughes Clarke (2003) described seven common sources of dynamic errors (there are others), including: motion-scaling; time delays in the motion sensor output; imperfect alignment of the roll/pitch axis with respect to the sonar reference frame; errors in the relative offsets of sensors in the ship's coordinate system (two types, static and dynamic); vertical ship motion close to or directly over an area with a large sound speed gradient; and rolling with imperfect sound speed measurements in the surface waters. He also described an approach for identifying the source of the error through the analysis of the behaviour of the depth profile across and along the swath with respect to the time series forcing functions derived from the motion sensor (i.e. the heave, pitch and roll records). A key to this analysis is the determination of whether artefacts or undulations in the swath profiles rise and fall together across the swath or whether the outer edges of the swath rise and fall while the centre of the swath does not (Hughes Clarke 2003). Those artefacts where the outer edges of the swaths are accentuated (flapping) are more probably related to sound speed or roll-related issues (Fig. 10e–g), whereas those that cause the entire swath to rise and fall together are more probably related to heave or other vertically driven sources.

SBES and sub-bottom/seismic-reflection profiling

Hyperbolae. Common artefacts in SBES, sub-bottom profiler and unmigrated seismic-reflection data are the hyperbolae that form over small objects or undulations in the seafloor or sub-bottom. When mapping areas with glacial landforms, hyperbolae typically occur in sub-bottom profiles acquired, for example, from iceberg-ploughed seafloor or across mega-scale glacial lineations, linked to their relatively narrow depression and ridge topography (Fig. 11). Given the lack of angular resolution and the relatively broad beam width of an SBES, the shortest range to within the beam footprint will be recorded as if it was always directly below the vessel. The closest distance to the object that the sonar records in the form of an echo will change as the ship moves (Fig. 12a). This distance will appear as a changing depth to the object. A narrow object (narrow pit or peak) will appear to widen as the ship moves past it. The end result is a characteristic hyperbolic shape on the echogram, where the object is located in the centre (Fig. 12b). A narrow depression will have a typical bow-tie reflection associated with it from this effect (Fig. 12c, d, f), whereas an upstanding object has a hyperbolic reflection (Fig. 12b). Hyperbolic artefacts often obscure the narrow peaks in the sub-bottom profiles of heavily iceberg-ploughed seafloors (Fig. 11b). The same relationship will also cause edge effects at the boundaries of larger features, such as troughs or topographic highs, distorting their true dimensions by as much as the beam width at that depth. The migration of entire seismic-reflection surveys only became a

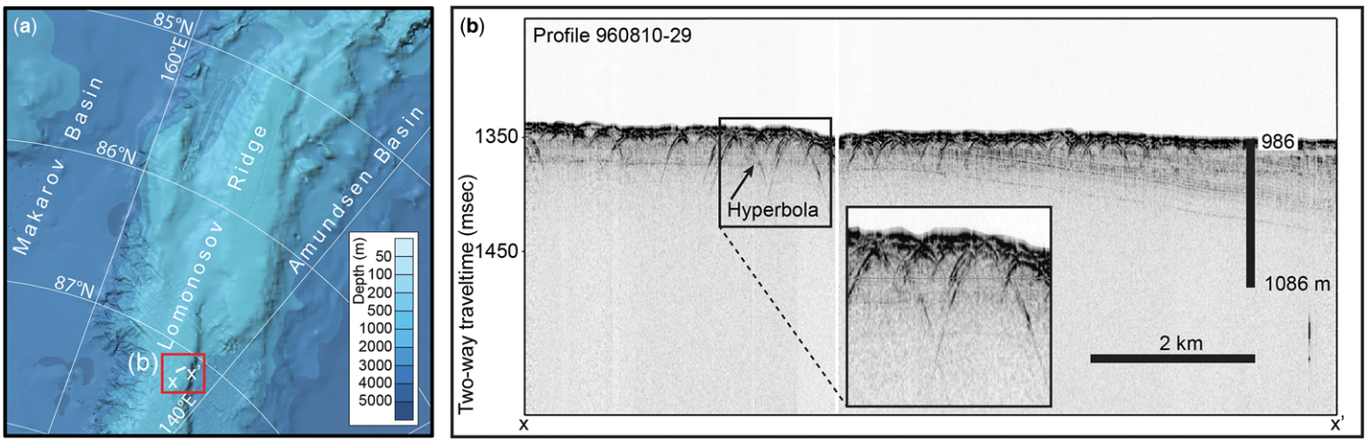

Fig. 11. Chirp sonar profile (**b**) from the crest of the Lomonosov Ridge, central Arctic Ocean (**a**), where an ice shelf is inferred to have grounded and produced glacial landforms closely resembling mega-scale glacial lineations (Jakobsson 1999; Jakobsson *et al.* 2016). The chirp profile was acquired with an EdgeTech SC-512 tow-fish and 100 ms long 2–4 kHz chirp pulse. The relatively narrow undulations in the seafloor are associated with marked hyperbolae.

practical option for academic research groups in the 1990s as a result of advances in processor and data storage capacity. Consequently, hyperbolae occur widely in older seismic-reflection data that have not been reprocessed.

Multiples. Multiples are common artefacts in sub-bottom profiles, referring to a situation in which a reflector appears in the profile multiple times instead of only at the TWT where the acoustic impedance contrast from two varying geological layers occurs. In other words, multiples of one specific reflector are occurring at the wrong locations in the profile. The most common cause of multiples is that the pulse, after being reflected back from the seafloor or sub-bottom reflector is, in turn, reflected by the sea surface to propagate a second (multiple) time down through the water column. The seabed most commonly gives the strongest echo and the first seabed multiple can be identified easily as an apparently strong reflection occurring consistently at twice the water depth and at double the slope (Fig. 12e). Multiples may also be generated by signal pulses bouncing repeatedly between the seafloor and a sub-seafloor reflector, or two sub-seafloor reflectors with strong acoustic impedance contrasts. Artefacts of this type are sometimes referred to as peg-leg multiples. In the worst cases, multiples of the seafloor and sub-bottom acoustic stratigraphy appear mixed with deeper real reflections, making interpretation difficult. A range of processing methods has been developed to suppress multiples in seismic-reflection data based on differences in their move-out with increasing source–receiver offsets relative to primary reflections, their periodicity or by modelling and subtraction.

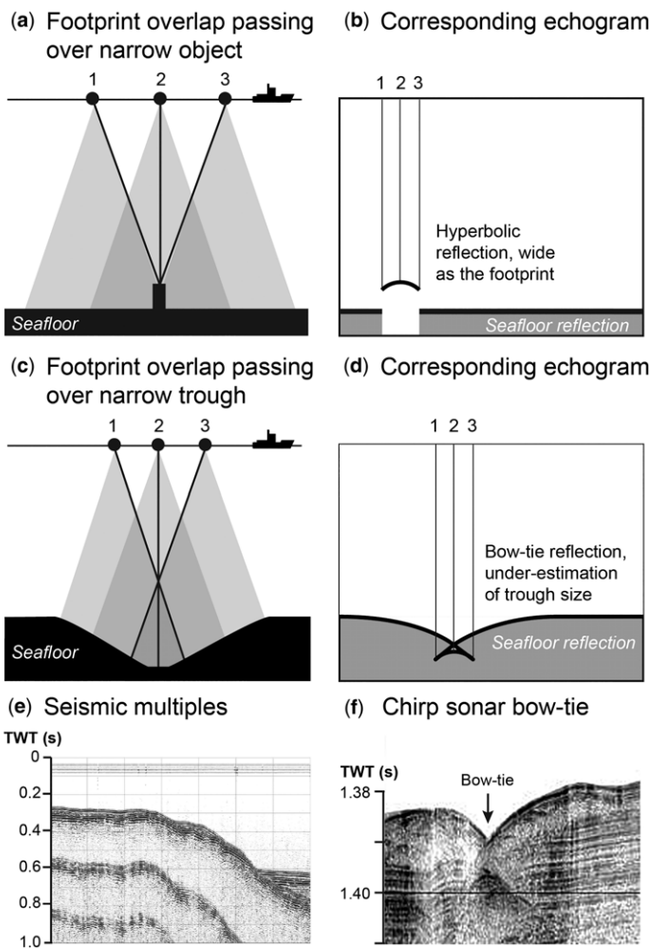

Fig. 12. Schematic illustrations of artefacts in the form of (**a**–**d, f**) hyperbolic echoes and (**e**) multiple reflections in a seismic-reflection profile.

Survey platforms

Surface platforms: ships

An SBES, measuring water depth, has traditionally been a vital part of the navigation and collision-avoidance systems of ships. In turn, MBESs have been regarded as an investigative tool for mapping the seafloor since their initial development and installation in the early 1960s, when General Instruments Corporation equipped US naval vessels with the Sonar Array Sounding System, which could obtain up to 61 soundings for each sonar pulse (Glen 1970). The company then developed the commercial SeaBeam system and equipped Australian, French and US government vessels; the first academic vessel to be fitted with SeaBeam belonged to the Scripps Institution of Oceanography (Glen 1976). MBESs are now available from several companies (e.g. Kongsberg, Atlas/Teledyna, Reson) and hundreds of research vessels worldwide, ranging in size from small boats (Kvitek 2016) to ocean-going research and mapping ships, are now equipped with multibeam sonar systems (see researchvessels.org).

Historically, the challenging ice and weather conditions encountered at high latitudes have limited seafloor mapping with conventional vessels to nearshore areas or seasonally ice-free zones (Paull *et al.* 2015). The acquisition of detailed planform data from the seafloor in polar waters thus required both ice-capable

research vessels and advancing multibeam technology. Regional mapping efforts have intensified at high latitudes and the last two decades have witnessed vessels of ice-breaking capability being equipped with multibeam sonar systems and deployed increasingly in polar waters where sea ice and icebergs are regular hazards (e.g. Armstrong *et al.* 2012). This has been for several reasons. First, as part of the commitments of signatory nations under the Antarctic Treaty System, significant scientific activity on land and/or at sea in Antarctica is required. Several nations have built and deployed ice-breaking or ice-strengthened vessels for both scientific and logistical use, and these ships are often operated by government-sponsored polar research laboratories. Examples include the ice-breakers IB *Oden*, RV *Polarstern*, USCGC *Healy* and RRS *James Clark Ross* operated by Sweden, Germany, the USA and UK, respectively. Second, mapping of high-latitude continental margins has been accelerated by the United Nations Convention on the Law of the Sea Article 76 concerning the determination and delineation of the outer limits of the extended continental shelf beyond 200 nautical miles from the coast and other rights of states over the continental shelf (Wood *et al.* 2011; Armstrong *et al.* 2012). Third, industrial interest in hydrocarbon exploration and exploitation in shelf seas formerly or presently affected by ice has also stimulated the acquisition of swath-bathymetric data along with conventional seismic-reflection and 3D seismic datasets – the Norwegian margin is a clear example. Although some of these datasets remain confidential to industry, a number have been released for academic use.

Collecting high-quality multibeam sonar data in ice-covered waters from an ice-breaker is not an easy task. The process of breaking ice produces noise that greatly degrades the ability to receive echoes from the seafloor, as does the scraping of broken ice along the ship's hull (where the transducers are located). To mitigate this situation it is best to use two ice-breakers, one leading to clear a path in the ice and the second equipped with an MBES instrument to follow in the cleared path and carry out the survey (Armstrong *et al.* 2012; Fig. 13a). In the absence of a second ice-breaker, several techniques have been developed to allow the collection of MBES data in the harsh ice conditions of the central Arctic Ocean. If the ice-breaker is very manoeuvrable, such as the Swedish ice-breaker *Oden*, it can break a clear area of ice and use the wide beam width of the MBES to ensonify a large circular area around the vessel as it does a 360° degree turn around its axis (a pirouette; Fig. 13b). This technique was first used during the Lomonosov Ridge of Greenland Expedition 2007, when mapping was carried out in 10/10ths sea ice conditions north of Greenland on the Morris Jesup Rise (Fig. 13c). Another strategy in the absence of a second ship is to monitor the shifting distribution of sea ice using remote sensing information and to exploit polynyas and leads within the ice-covered region as they develop. A survey over a large area on the inner part of the Amundsen Sea continental shelf was conducted within a polynya in 2006 (Larter *et al.* 2009) and a broad corridor along the Filchner Ice Shelf front was surveyed in 2011 by operating in a shore lead that was only open for four days (Larter *et al.* 2012).

Some modern MBES systems also offer the opportunity to tilt the direction of their transmit beam forward or aft. For less manoeuvrable ships, this allows the vessel to stay in one place and sweep the beam forward and aft (like the hokey-pokey dance) allowing for high-quality data to be collected several kilometres ahead and behind the vessel (Fig. 13d, e). Both these approaches make for very slow data acquisition, but do allow the collection of reasonable quality data by a single ship in harsh ice conditions.

Subsurface platforms: ROVs and AUVs

Subsurface platforms have been in use for decades in marine research and seafloor mapping (Geyer 1977). The collective term 'unmanned underwater vehicle' includes: first, non-autonomous ROVs, which are controlled and powered from the surface by an operator/pilot via an umbilical cable usually containing a fibre optic link or using remote control; and, second, AUVs, which are machines that travel underwater without real-time operator guidance or instruction, usually being pre-programmed prior to launch. Both ROVs and AUVs were initially developed, in part at least, for industrial and military use, as well as for civilian mapping and scientific investigations.

ROVs and AUVs of varying sophistication have been deployed in areas of the Arctic and Antarctic that are too difficult or dangerous to survey or cannot be accessed by surface vessels. The underside of extensive sea ice fields and the huge water-filled cavities beneath floating ice shelves are clear examples (e.g. Powell *et al.* 1996; Wadhams *et al.* 2006; Dowdeswell *et al.* 2008; Jenkins *et al.* 2010). ROVs, flying close to the seafloor, can provide high-resolution multibeam imagery of, for example, sediments, landforms and the accompanying surface biota, and some also have a shallow sub-bottom profiling capability (e.g. Graham *et al.* 2013).

The utilization of AUVs at high latitudes began 20 years ago with the deployment of 200 km of fibre optic cable beneath ice-covered waters in the Canadian Arctic (McFarlane & Murphy 2013). AUVs equipped with multibeam sonar can be deployed relatively close to the seafloor, thus providing a finer horizontal resolution than surface sonar systems and revealing greater bathymetric detail. Such devices have been deployed many times in, for example, the Canadian United Nations Convention on the Law of the Sea mapping programme (Millar & Mackay 2015). Today AUVs also deploy multibeam systems in the upward-looking mode to map the underside of floating sea ice and ice shelves (Dutrieux *et al.* 2016; Wilkinson & Wadhams 2016) as well in the more conventional downward-looking configuration to map the seafloor and its component submarine landforms (e.g. Graham *et al.* 2013).

Subsurface platforms: submarines

In 1931, the submarine *Nautilus* was used to obtain oceanographic information beneath sea ice during cruises in Arctic waters (Wilkins 1931). Although *Nautilus* never reached its intended destination of the North Pole, it demonstrated the concept of using submarines for exploration underneath a sea ice canopy (Nasht 2005). The first operational nuclear submarine, also named *Nautilus* (USS *Nautilus*; SSN-571), reached the sea ice covered North Pole on 3 August 1958. More recently, some military submarines (particularly nuclear submarines) have been equipped intermittently with upward-looking SBES systems and, later, imaging side-scan sonar systems to investigate the thickness and detailed subsurface shape of the extensive canopy of sea ice covering much of the Arctic Ocean (e.g. Williams *et al.* 1975; McLaren *et al.* 1984; Wadhams 1988). Since 1993, the US Navy has made a series of unclassified nuclear submarine cruises to the Arctic for scientific research through the Science Ice Exercises (SCICEX) programme. Three of these cruises conducted surveys of portions of the Gakkel Ridge. Swath-bathymetric data were acquired by, for example, the USS *Hawksbill* utilizing the Seafloor Characterization and Mapping Pods geophysical instrument package, which was installed for the 1998 and 1999 cruises (Edwards *et al.* 2001; Edwards & Coakley 2003). However, the geophysical mapping data acquired by submarines suffers from the difficulties of accurately navigating underwater, particularly beneath sea ice, making surfacing to acquire GPS fixes a cumbersome operation. Analyses of swath bathymetry from crossing tracks of the SCICEX-98 and SCICEX-99 cruises revealed that the horizontal accuracy was within *c.* 2 km and that the error increased as a function of time since the last acquired GPS fix (Edwards & Coakley 2003). This implies clearly visible artefacts when the swath bathymetry and side-scan data from Seafloor Characterization and Mapping Pods are being brought together (Edwards & Coakley 2003) or merged with other data acquired from surface vessels (Kurras *et al.* 2001).

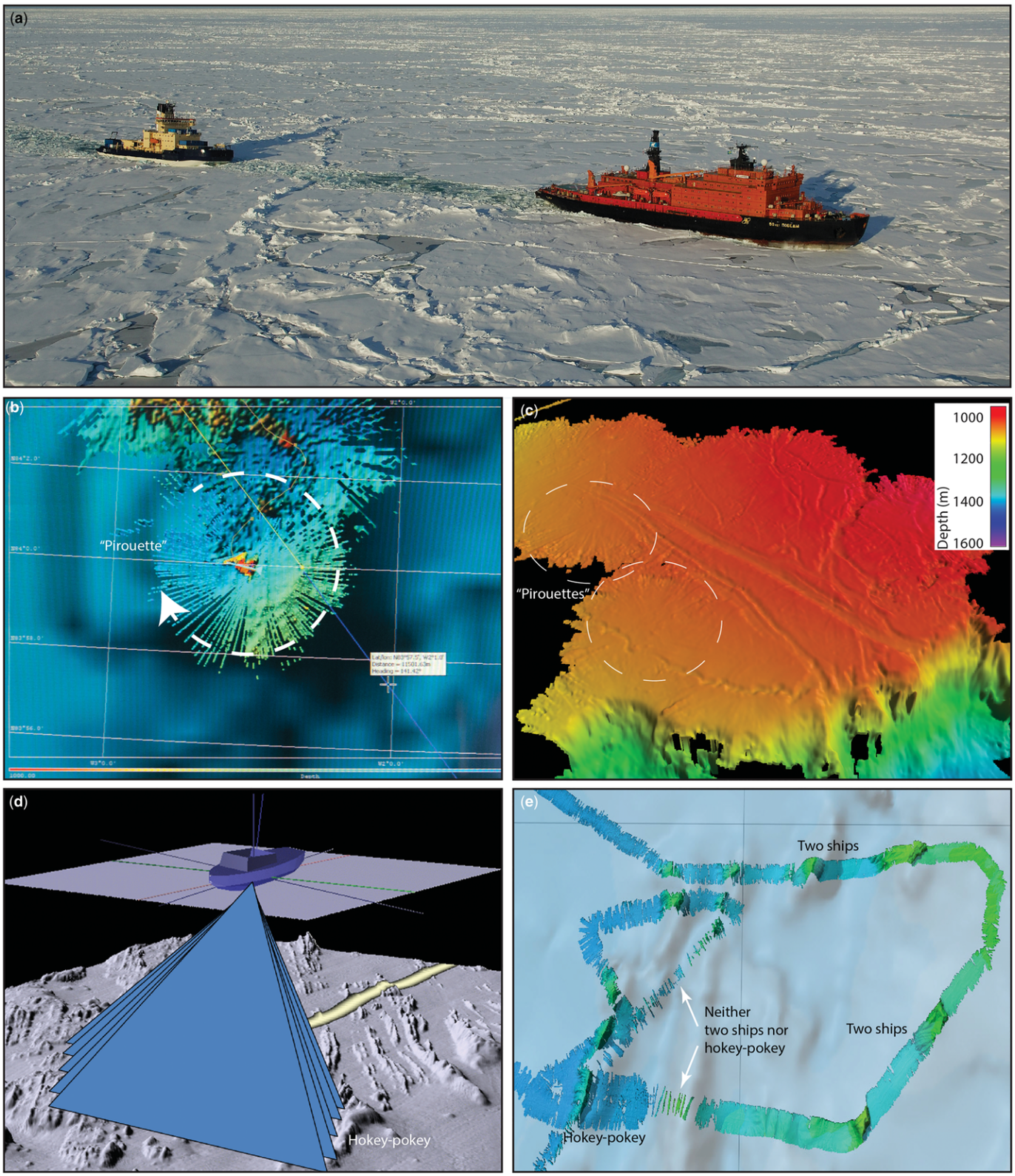

Fig. 13. (**a**) A two-ship operation in severe sea ice conditions north of Greenland during the Lomonosov Ridge of Greenland (LOMROG) 2007 expedition. The Russian nuclear ice-breaker *50 Years of Victory* is clearing a path for Swedish ice-breaker *Oden*. (**b**) Screen shot of multibeam acquisition by *Oden* carrying out a pirouette during the LOMROG 2007 expedition in 10/10ths sea ice cover on the Morris Jesup Rise north of Greenland. (**c**) The crest of Morris Jesup Rise mapped by assembling several pirouettes in a mosaic of multibeam data. (**d**) The concept of the hokey-pokey acquisition methods that can be applied in severe sea ice conditions. (**e**) Multibeam data acquired in heavy ice conditions by ice-breakers USCGC *Healy* and CCGS *Louis S. St-Laurent* in the Canadian Basin, central Arctic Ocean, using two-ship and hokey-pokey acquisition methods.

Conclusions

We have outlined the main methods by which the shape of the seafloor and the stratigraphy of the material that underlies it have been investigated. It is clear that major technological innovations, often driven initially by military and industrial considerations, have greatly enhanced the capability for imaging the seafloor and mapping the marine stratigraphic record.

In particular, the development of MBES methods to produce high-resolution digital elevation models of the seafloor has allowed the acquisition of the images of many high-latitude areas illustrated and discussed in the *Atlas of Submarine Glacial Landforms*. The horizontal resolution of these data varies from a few tens of metres in deep water to a few metres or even better in shallower water using relatively high-frequency narrow beam systems. The advent of ice-breaking research vessels as platforms for the deployment of MBES systems in Arctic and Antarctic waters has also been vital.

The increasing availability of 3D seismic-reflection data from northern high-latitude shelves has also allowed the mapping of glacial landforms on the palaeosurfaces of buried continental shelves. This is a growing area of research, increasingly stimulated as 3D data are released to the wider academic community by industry. Traditional shallow SBPs and 2D seismic-reflection datasets continue to provide important stratigraphic information, which is combined with landform mapping to provide the fullest possible description of the geometry of submarine glacial landforms.

The application of these planview and stratigraphic geophysical datasets to the understanding of glacial landforms and the implications for the reconstruction of past ice-sheet extent and dynamics is the topic of the following sections of the *Atlas*, to which this technical discussion provides important background in the form of a physical explanation of the operation of echo sounders and seismic systems, together with some of the problems associated with them.

References

Andreassen, K., Nilssen, L.-C., Rafaelsen, B. & Kuilman, L. 2004. Three-dimensional seismic data from the Barents Sea margin reveal evidence of past ice streams and their dynamics. *Geology*, **32**, 729–732.

Andreassen, K., Ødegaard, C.M. & Rafaelsen, B. 2007. Imprints of former ice streams, imaged and interpreted using industry three-dimensional seismic data from the south-western Barents Sea. *In*: Davies, R.J., Posamentier, H.W., Wood, I.L. & Cartwright, J.A. (eds) *Seismic Geomorphology: Applications to Hydrocarbon Exploration and Production*. Geological Society, London, Special Publications, **277**, 151–169, http://doi.org/10.1144/GSL.SP.2007.277.01.09

Armstrong, A.A., Mayer, L.A. & Mosher, D.C. 2012. Gathering multibeam bathymetry aboard icebreakers: US-Canada joint expedition deploys *Healy* and *Louis S. St-Laurent* for extended continental shelf mapping in Arctic Ocean. *Sea Technology Magazine*, October, 10–13.

Arndt, J.E., Schenke, H.W. *et al.* 2013. The International Bathymetric Chart of the Southern Ocean (IBCSO) Version 1.0 – a new bathymetric compilation covering circum-Antarctic waters. *Geophysical Research Letters*, **40**, 3111–3117.

Ashcroft, W. 2011. *A Petroleum Geologist's Guide to Seismic Reflection*. Wiley-Blackwell, Oxford.

Barnes, P.W. & Lien, R. 1988. Iceberg rework shelf sediments to 500 m off Antarctic. *Geology*, **16**, 1130–1133.

Barrie, J.V. 1980. Iceberg–seabed interaction (Northern Labrador Sea). *Annals of Glaciology*, **1**, 71–76.

Belderson, R.H. & Wilson, J.B. 1973. Iceberg plough marks in the vicinity of the Norwegian Trough. *Norsk Geologisk Tidsskrift*, **53**, 323–328.

Belderson, R.H., Kenyon, N.H., Stride, A.H. & Stubbs, A.R. 1972. *Sonographs of the Seafloor*. Elsevier, Amsterdam.

Berndt, C., Costa, S., Canals, M., Camerlenghi, A., De Mol, B. & Saunders, M. 2012. Repeated slope failure linked to fluid migration: the Ana submarine landslide complex, Eivissa Channel, Western Mediterranean Sea. *Earth and Planetary Science Letters*, **319–320**, 65–74.

Blackington, J.G., Hussong, D.M. & Kosalos, J.G. 1983. First results from a combination side-scan sonar and seafloor mapping system (SeaMarc II). *Proceeding of Offshore Technology Conference*, 2–5 May, Houston, 307–314, http://doi.org/10.4043/4478-MS

Blondel, P. 2009. *The Handbook of Sidescan Sonar*. Springer Science & Business Media, Chichester.

Brookshire, B.N., Jr, Landers, F.P. & Stein, J.A. 2015. Applicability of ultra-high-resolution 3D seismic data for geohazard identification at mid-slope depths in the Gulf of Mexico: initial results. *Underwater Technology*, **32**, 271–278.

Bünz, S., Mienert, J., Bryn, P. & Berg, K. 2005. Fluid flow impact on slope failure from 3D seismic data: a case study in the Storegga Slide. *Basin Research*, **17**, 109–122.

Bünz, S., Polyanov, S., Vadakkepuliyambatta, S., Consolaro, C. & Mienert, J. 2012. Active gas venting through hydrate-bearing sediments on the Vestnesa Ridge, offshore W-Svalbard. *Marine Geology*, **332–334**, 189–197.

Canals, M., Urgeles, R. & Calafat, A.M. 2000. Deep sea-floor evidence of past ice streams off the Antarctic Peninsula. *Geology*, **28**, 31–34.

Clark, C.D. & Spagnolo, M. 2016. Glacially eroded cross-shelf troughs surrounding Iceland from Olex data. *In*: Dowdeswell, J.A., Canals, M., Jakobsson, M., Todd, B.J., Dowdeswell, E.K. & Hogan, K.A. (eds) *Atlas of Submarine Glacial Landforms: Modern, Quaternary and Ancient*. Geological Society, London, Memoirs, **46**, 165–166, http://doi.org/10.1144/M46.86

Cleveland, C.J. & Morris, C.G. 2014. *Handbook of Energy: Chronologies, Top Ten Lists, and Word Clouds*. Elsevier, Amsterdam.

Damuth, J.E. 1978. Echo character of the Norwegian–Greenland Sea: relationship to Quaternary sedimentation. *Marine Geology*, **28**, 1–36.

de Moustier, C. & Kleinrock, M.C. 1986. Bathymetric artifacts in Sea Beam data: how to recognize them and what causes them. *Journal of Geophysical Research, Solid Earth*, **91**, 3407–3424.

Donovan, D.T. & Stride, A.H. 1961. An acoustic survey of the sea floor south of Dorset and its geological interpretation. *Philosophical Transactions of the Royal Society, London*, **B244**, 299–330.

Dove, D., Polyak, L. & Coakley, B. 2014. Widespread, multi-source glacial erosion on the Chukchi margin, Arctic Ocean. *Quaternary Science Reviews*, **92**, 112–122.

Dowdeswell, J.A. & Hogan, K.A. 2016. Huge iceberg ploughmarks and associated corrugation ridges on the northern Svalbard shelf. *In*: Dowdeswell, J.A., Canals, M., Jakobsson, M., Todd, B.J., Dowdeswell, E.K. & Hogan, K.A. (eds) *Atlas of Submarine Glacial Landforms: Modern, Quaternary and Ancient*. Geological Society, London, Memoirs, **46**, 269–270, http://doi.org/10.1144/M46.4

Dowdeswell, J.A. & Ottesen, D. 2013. Buried iceberg ploughmarks in the Early Quaternary sediments of the central North Sea: a two million year record of glacial influence from 3D seismic data. *Marine Geology*, **344**, 1–9.

Dowdeswell, J.A. & Ottesen, D. 2016. Three-dimensional seismic imagery of deeply buried iceberg ploughmarks in North Sea sediments. *In*: Dowdeswell, J.A., Canals, M., Jakobsson, M., Todd, B.J., Dowdeswell, E.K. & Hogan, K.A. (eds) *Atlas of Submarine Glacial Landforms: Modern, Quaternary and Ancient*. Geological Society, London, Memoirs, **46**, 291–292, http://doi.org/10.1144/M46.53

Dowdeswell, J.A., Ottesen, D. & Rise, L. 2006. Flow-switching and large-scale deposition by ice streams draining former ice sheets. *Geology*, **34**, 313–316.

Dowdeswell, J.A., Evans, J. *et al.* 2008. Autonomous underwater vehicles (AUVs) and investigations of the ice–ocean interface in Antarctic and Arctic waters. *Journal of Glaciology*, **54**, 661–672.

Dutrieux, P., Jenkins, A. & Nicholls, K.W. 2016. Ice-shelf basal morphology from an upward-looking multibeam system deployed from an autonomous underwater vehicle. *In*: Dowdeswell, J.A., Canals,

M., Jakobsson, M., Todd, B.J., Dowdeswell, E.K. & Hogan, K.A. (eds) *Atlas of Submarine Glacial Landforms: Modern, Quaternary and Ancient*. Geological Society, London, Memoirs, **46**, 219–220, http://doi.org/10.1144/M46.79

Edelmann, H. 1968. An underwater sound source with higher seismic efficiency. *Geophysical Prospecting*, **16**, 474–490.

Edgerton, H.F. & Hayward, E.C. 1964. The Boomer sonar source for seismic profiling. *Journal of Geophysical Research*, **69**, 3033–3042.

Edwards, M.H. & Coakley, B.J. 2003. SCICEX investigations of the Arctic Ocean system. *Chemie der Erde*, **63**, 281–328.

Edwards, M.H., Kurras, G.J., Tolstoy, M., Bohnenstiehl, D.R., Coakley, B.J. & Cochran, J.R. 2001. Evidence of recent volcanic activity on the ultra-slow spreading Gakkel Ridge. *Nature*, **409**, 808–812.

Farr, H.K. 1980. Multi-beam bathymetric sonar: SEA BEAM and HYDRO CHART. *Marine Geodesy*, **4**, 77–93.

Fish, J.P. & Carr, H.A. 2001. *Sound Reflection: Advanced Applications of Side Scan Sonar Data*. Lower Cape Publishing, Orleans, Massachusetts.

Fonseca, L. & Mayer, L.A. 2007. Remote estimation of surficial seafloor properties through the application Angular Range Analysis to multibeam sonar data. *Marine Geophysical Researches*, **28**, 119–126.

Geyer, R.A. (ed.) 1977. *Submersibles and their Use in Oceanography and Ocean Engineering*. Elsevier Oceanography Series, **17**. Elsevier, Amsterdam.

Glen, M.F. 1970. Introducing an operational multi-beam-array sonar. *International Hydrographic Review*, **47**, 35–40.

Glen, M.F. 1976. Multi-narrow beam systems. The Marine Technology Society and the Oceanic Engineering Society of the Institute of Electrical and Electronic Engineers, *Proceedings Oceans 1976*, 13–15 September, Washington, DC, 8D-1–8D-2.

Graham, A.G.C., Fretwell, P.T., Larter, R.D., Hodgson, D.A., Wilson, C.K., Tate, A.J. & Morris, P. 2008. A new bathymetric compilation highlighting extensive paleo-ice sheet drainage on the continental shelf, South Georgia, sub-Antarctica. *Geochemistry, Geophysics, Geosystems*, **9**, http://doi.org/10.1029/2008GC001993

Graham, A.G.C., Dutrieux, P. *et al.* 2013. Seabed corrugations beneath an Antarctic ice shelf revealed by autonomous underwater vehicle survey: origin and implications for the history of Pine Island Glacier. *Journal of Geophysical Research: Earth Surface*, **118**, 1356–1366.

Harris, I.McK. & Jollymore, P.G. 1974. Iceberg furrow marks on the continental shelf northeast of Bell Isle, Newfoundland. *Canadian Journal of Earth Sciences*, **11**, 43–52.

Heezen, B.C., Tharp, M. & Ewing, M. 1959. *The Floors of the Oceans: I. The North Atlantic*. Geological Society of America, Special Papers, 65.

Holtedahl, H. & Sellevoll, M. 1971. *Geology of the Continental Margin of Eastern Norwegian Sea and the Skagerrak*. Institute of Geological Sciences Report 70/14.

Hughes Clarke, J.E. 2003. Dynamic motion residuals in swath sonar data: ironing out the creases. *International Hydrographic Review*, **4**, 6–23.

Hughes Clarke, J.E. 2015. Multispectral acoustic backscatter from multibeam, improved classification potential. *Proceedings of the US Hydrographic Conference*, 15–19, March, National Harbor, Maryland, USA, https://www.thsoa.org/references

Hunkins, K., Herron, T., Kutschale, H. & Peter, G. 1962. Geophysical studies of the Chukchi Cap, Arctic Ocean. *Journal of Geophysical Research*, **67**, 235–247.

International Hydrographic Organization 2005. *Manual on Hydrography*. 1st edn. International Hydrographic Organization Publications, C-13.

Jakobsson, M. 1999. First high-resolution chirp sonar profiles from the central Arctic Ocean reveal erosion of Lomonsov Ridge sediments. *Marine Geology*, **158**, 111–123.

Jakobsson, M. & Anderson, J.B. 2016. Corrugation ridges in the Pine Island Bay glacier trough, West Antarctica. *In*: Dowdeswell, J.A., Canals, M., Jakobsson, M., Todd, B.J., Dowdeswell, E.K. & Hogan, K.A. (eds) *Atlas of Submarine Glacial Landforms: Modern, Quaternary and Ancient*. Geological Society, London, Memoirs, **46**, 265–266, http://doi.org/10.1144/M46.5

Jakobsson, M., Gardner, J.V. *et al.* 2005. Multibeam bathymetric and sediment profiler evidence for ice grounding on the Chukchi Borderland, Arctic Ocean. *Quaternary Research*, **63**, 150–160.

Jakobsson, M., Anderson, J.B. *et al.* 2011. Geological record of ice shelf breakup and grounding line retreat, Pine Island Bay, West Antarctica. *Geology*, **39**, 691–694.

Jakobsson, M., Mayer, L. *et al.* 2012. The International Bathymetric Chart of the Arctic Ocean (IBCAO) Version 3.0. *Geophysical Research Letters*, **39**, http://doi.org/10.1029/2012GL052219

Jakobsson, M., Nilsson, J. *et al.* 2016. Evidence for an ice shelf covering the central Arctic Ocean during the penultimate glaciation. *Nature Communications*, **7**, http://doi.org/10.1038/ncomms10365

Jenkins, A., Dutrieux, P., Jacobs, S.S., McPhail, S.D., Perret, J.R., Webb, A.T. & White, D. 2010. Observations beneath Pine Island Glacier in West Antarctica and implications for its retreat. *Nature Geoscience*, **3**, 468–472.

Jones, E.J.W. 1999. *Marine Geophysics*. Wiley, London.

Kallweit, R.S. & Wood, L.C. 1982. The limits of resolution of zero-phase wavelets. *Geophysics*, **47**, 1035–1046.

King, L.H. 1969. Submarine end moraines and associated deposits on the Scotian Shelf. *Geological Society of America Bulletin*, **80**, 83–96.

Klepsvik, J.O. & Fossum, B.A. 1980. Studies of icebergs, ice fronts and ice walls using side-scanning sonar. *Annals of Glaciology*, **1**, 31–36.

Kurras, G.J., Edwards, M.H. *et al.* 2001. Comparison of Seabeam 2112 and SCAMP bathymetry data along the Gakkel Ridge: preliminary mapping results from the Healy 0102 Arctic cruise. *Proceedings of the MTS/IEEE Conference and Exhibition 3*, 6–9 November 2001, Honolulu, Hawaii, 1496–1499.

Kvitek, R. 2016. Seafloor Mapping Lab: Capabilities-R/V *Kelpfly*, http://seafloor.otterlabs.org/descriptions/kelpflydescrip.html

Lafuerza, S., Sultan, N. *et al.* 2012. Failure mechanisms of Ana Slide from geotechnical evidence, Eivissa Channel, Western Mediterranean Sea. *Marine Geology*, **307**, 1–21.

Larter, R.D., Graham, A.G.C. *et al.* 2009. Subglacial bedforms reveal complex basal regime in a zone of paleo-ice stream convergence, Amundsen Sea embayment, West Antarctica. *Geology*, **37**, 411–414.

Larter, R.D., Graham, A.G.C., Hillenbrand, C.-D., Smith, J.A. & Gales, J.A. 2012. Late Quaternary grounded ice extent in the Filchner Trough, Weddell Sea, Antarctica: new marine geophysical evidence. *Quaternary Science Reviews*, **53**, 111–122.

Leenhardt, O. 1972. *Le sondage sismique continu*. Masson & Cie, Paris.

Lien, R.L. 1981. Seabed features in the Blaaenga area, Weddell Sea, Antarctica, POAC 81. *The Sixth International Conference on Port and Ocean Engineering under Arctic Conditions*, 27–31 July, Quebec, Canada, 706–716.

Loncarevic, B.D., Courtney, R.C. *et al.* 1994. Songraphy of a glaciated continental shelf. *Geology*, **22**, 747–750.

Lurton, X. 2010. *An Introduction to Underwater Acoustics: Principles and Applications*. 2nd edn. Springer Science & Business Media, London, New York.

Mackenzie, K.V. 1981. Nine-term equation for the sound speed in the oceans. *Journal of Acoustical Society America*, **70**, 807–812.

Mayer, L.A. 1979. The origin of fine-scale acoustic stratigraphy in deep-sea carbonates. *Journal of Geophysical Research*, **84**, 6177–6184.

Mayer, L.A., Paton, C.W., Gee, L., Gardner, J.V. & Ware, C.W. 2000. Interactive 3-D visualization: a tool for seafloor navigation, exploration, and engineering. *Proceedings of the IEEE Oceans*, **2**, 913–920.

McAdoo, D. & Laxon, S. 1997. Antarctic tectonics: constraints from an ERS-1 Satellite Marine Gravity Field. *Science*, **276**, 556–560.

McFarlane, J. & Murphy, R.F. 2013. AUVs survey the Canadian Arctic: ISE's Arctic AUVs evolve to conduct under-ice missions. *Sea Technology*, May, 41–43.

McLaren, A.S., Wadhams, P. & Weintraub, R. 1984. The sea ice topography of M'Clure Strait in winter and summer of 1960 from submarine profiles. *Arctic*, **37**, 110–120.

Millar, G. & Mackay, L. 2015 . Maneuvering under the ice: AUV development in the Arctic. *Sea Technology*, April, 35–38.

Mosher, D.C. & Simpkin, P.G. 1999. Environmental marine geoscience 1. Status and trends of marine high-resolution seismic reflection profiling: data acquisition. *Geoscience Canada*, **26**, 174–188.

Nasht, S. 2005. *Last Explorer: Hubert Wilkins, Hero of the Golden Age of Polar Exploration*. Hodder Australia.

Newton, G.B. 2000. The science ice exercise program: history, achievement, and future of SCICEX. *Arctic Research of the United States*, **14**, 2–7.

Nyquist, H. 1928. Certain topics in telegraph transmission theory. *Transactions of the American Institute of Electrical Engineers*, **47**, 617–644.

Parkes, G. & Hatton, L. 1986. *The Marine Seismic Source*. D. Reidel, Dordrecht.

Paull, C.K, Dallimore, D.W. *et al.* 2015. Active mud volcanoes on the continental slope of the Canadian Beaufort Sea. *Geochemistry, Geophysics, Geosystems*, **16**, 3160–3181.

Perez-Garcia, C., Berndt, C. *et al.* 2011. Linked halokinesis and mud volcanism at the Mercator mud volcano, Gulf of Cadiz. *Journal of Geophysical Research*, 116, http://doi.org/10.1029/2010JB008061

Petersen, C.J., Bünz, S., Hustoft, S., Mienert, J. & Klaeschen, D. 2010. High-resolution P-Cable 3D seismic imaging of gas chimney structures in gas hydrated sediments of an Arctic sediment drift. *Marine and Petroleum Geology*, **27**, 1981–1994.

Planke, S., Berndt, C., Mienert, J. & Bünz, S. 2009*a*. P-Cable High-Resolution 3D Seismic Acquisition Technology. *INVEST 2009 Workshop*, 23–25 September, University of Bremen, Bremen, Germany.

Planke, S., Eriksen, F.N., Berndt, C., Mienert, J. & Masson, D.G. 2009*b*. P-Cable high-resolution seismic. *Oceanography*, **22**, 85.

Polyak, L., Edwards, M.H. *et al.* 2001. Ice shelves in the Pleistocene Arctic Ocean inferred from glaciogenic deep-sea bedforms. *Nature*, **410**, 453–459.

Powell, R.D., Dawber, M., McInnes, J.N. & Pyne, A. 1996. Observations of the grounding-line area at a floating glacier terminus. *Annals of Glaciology*, **22**, 217–223.

Pudsey, C.J., Barker, P.F. & Larter, R.D. 1994. Ice sheet retreat from the Antarctic Peninsula shelf. *Continental Shelf Research*, **14**, 1647–1675.

Reddy, P.R. 2012. Historical development of seismic imaging technique – an overview. *Journal of the Indian Geophysical Union*, **16**, 71–86.

Renard, V. & Allenou, J.P. 1979. SeaBeam multibeam echo sounding. *In*: Charcot, J. (ed.) *Description, Evaluation and First Results*. *International Hydrographic Review*, **56**, 35–67.

Ryan, J.C., Dowdeswell, J.A. & Hogan, K.A. 2016. Three cross-shelf troughs on the continental shelf of SW Greenland from Olex data. *In*: Dowdeswell, J.A., Canals, M., Jakobsson, M., Todd, B.J., Dowdeswell, E.K. & Hogan, K.A. (eds) *Atlas of Submarine Glacial Landforms: Modern, Quaternary and Ancient*. Geological Society, London, Memoirs, **46**, 167–168, http://doi.org/10.1144/M46.9

Sandwell, D.T., Smith, W.H.F., Gille, S., Jayne, S., Soofi, & Coakley, B. 2001. Bathymetry from Space: White paper in support of a high-resolution, ocean altimeter mission. Online white paper, http://topex.ucsd.edu/marine_grav/white_paper.pdf

Schock, S.G., LeBlanc, L.R. & Mayer, L.A. 1989. Chirp subbottom profiler for quantitative sediment analysis. *Geophysics*, **54**, 445–450.

Sellevoll, M.A. & Sundvor, E. 1974. The origin of the Norwegian Channel – a discussion based on seismic measurements. *Canadian Journal of Earth Sciences*, **11**, 224–231.

Sheriff, R.E. 1996. Understanding the Fresnel Zone. *AAPG Explorer (Geophysical Corner)*, October, 18–19.

Sheriff, R.E. & Geldart, L.P. 1995. *Exploration Seismology*. 2nd edn. Cambridge University Press, Cambridge.

Shipley, T.H., McIntosh, K.D., Silver, E.A. & Stoffa, P.L. 1992. Three-dimensional seismic imaging of the Coast Rica Accretionary Prism: structural diversity in a small volume of the lower slope. *Journal of Geophysical Research*, **97**, 4439–4459.

Simpkin, P.G. 2005. The Boomer sound source as a tool for shallow water geophysical exploration. *Marine Geophysical Researches*, **204**, 171–181.

Smith, W.H.F. & Sandwell, D.T. 1997. Global seafloor topography from satellite altimetry and ship depth soundings. *Science*, **277**, 1957–1962.

Somers, M.L., Carson, R.M., Revie, J.A., Edge, R.H., Barrows, B.J. & Andrews, A.G. 1978. GLORIA II – an improved long range sidescan sonar. *In*: *Proceedings of the Institute of Electrical Engineering on Offshore Instrumentation and Communications*. Oceanology International Technical Session J. BPS Publications, London, 16–24.

Stewart, M.A. 2016. Assemblage of buried and seabed tunnel valleys in the central North Sea: from morphology to ice-sheet dynamics. *In*: Dowdeswell, J.A., Canals, M., Jakobsson, M., Todd, B.J., Dowdeswell, E.K. & Hogan, K.A. (eds) *Atlas of Submarine Glacial Landforms: Modern, Quaternary and Ancient*. Geological Society, London, Memoirs, **46**, 317–320, http://doi.org/10.1144/M46.140

Stewart, M.A., Lonergan, L. & Hampson, G. 2013. 3D seismic analysis of buried tunnel valleys in the central North Sea: morphology, cross-cutting generations and glacial history. *Quaternary Science Reviews*, **72**, 1–17.

Stride, A.H. 1960. Recognition of folds and faults on rock surfaces beneath the sea. *Nature*, **185**, 837.

Stride, A.H. 1992. The first geological use of side-scan sonar. *Geology Today*, **8**, 146–150.

Tucker, M.J. 1961. Beam identification in multiple beam echo-sounders. *International Hydrographic Review*, **38**, 25–32.

Urick, R.J. 1983. *Principles of Underwater Sound*. McGraw-Hill, New York.

Upadhyay, S.K. 2004. *Seismic Reflection Processing*. Springer, Berlin.

Vadakkepuliyambatta, S., Bünz, S., Tasianas, A. & Mienert, J. 2016. Iceberg ploughmarks in the SW Barents Sea imaged using high-resolution P-Cable 3D seismic data. *In*: Dowdeswell, J.A., Canals, M., Jakobsson, M., Todd, B.J., Dowdeswell, E.K. & Hogan, K.A. (eds) *Atlas of Submarine Glacial Landforms: Modern, Quaternary and Ancient*. Geological Society, London, Memoirs, **46**, 281–282, http://doi.org/10.1144/M46.113

Vail, P.R., Mitchum, R.M. & Thompson, S. 1977. Seismic stratigraphy and global changes of sea level, Part 3 – Relative changes of sea level from coastal onlap. *In*: Payton, C.E. (ed.) *Seismic Stratigraphy – Applications to Hydrocarbon Exploration*. American Association of Petroleum Geologists, Memoirs, **26**, 63–81.

Vogt, P.R. & Tucholke, B.E. 1986. Imaging the ocean floor: history and state of the art. *In*: Vogt, P.R. & Tucholke, B.E. (eds) *The Geology of North America, Volume M, The Western North Atlantic Region*. Geological Society of America, Boulder, 19–44.

Wadhams, P. 1978. Sidescan sonar imagery of sea ice in the Arctic Ocean. *Canadian Journal of Remote Sensing*, **4**, 161–173.

Wadhams, P. 1988. The underside of Arctic sea ice imaged by sidescan sonar. *Nature*, **333**, 161–164.

Wadhams, P., Wilkinson, J.P. & McPhail, S.D. 2006. A new view of the underside of Arctic sea ice. *Geophysical Research Letters*, **33**, http://doi.org/10.1029/2005GL025131

Ware, C. 1989. Fast hill shading with cast shadows. *Computers & Geosciences*, **15**, 1327–1334.

Weatherall, P., Marks, K.M. *et al.* 2015. A new digital bathymetric model of the world's oceans. *Earth and Space Science*, **2**, 331–345.

Wilkins, H. 1931. *Under the North Pole: the Wilkins–Ellsworth Submarine Expedition*. Brewer, Warren & Putnam, New York.

Wilkinson, J.P. & Wadhams, P. 2016. The three-dimensional shape of sea ice revealed by multibeam sonar. *In*: Dowdeswell, J.A., Canals, M., Jakobsson, M., Todd, B.J., Dowdeswell, E.K. & Hogan, K.A. (eds) *Atlas of Submarine Glacial Landforms: Modern, Quaternary and Ancient*. Geological Society, London, Memoirs, **46**, 303–304, http://doi.org/10.1144/M46.181

Williams, E., Swithinbank, C.W.M. & Robin, G. de Q. 1975. A submarine sonar study of Arctic pack ice. *Journal of Glaciology*, **15**, 349–365.

Wille, P. 2005. *Sound Images of the Ocean in Research and Monitoring*. Springer, Berlin.

Wood, L., Henrys, S.A., Stagpoole, V., Davy, B. & Wright, I. 2011. Legal continental shelf. *In*: Gupta, H.K. (ed.) *Encyclopedia of Solid Earth Geophysics*. Springer, Berlin, 669–675.

Zhou, H. 2014. *Practical Seismic Data Processing*. Cambridge University Press, Cambridge.